Master Thesis
TVVR 18/5006

Soil moisture modeling for agricultural needs in Brazil, France, and the U.S.A.

Filipe Fava

Division of Water Resources Engineering
Department of Building and Environmental Technology
Lund University

Soil moisture modeling for agricultural needs in Brazil, France, and the U.S.A.

By:
Filipe Fava

Master Thesis

Division of Water Resources Engineering
Department of Building & Environmental Technology
Lund University
Box 118
221 00 Lund, Sweden

Water Resources Engineering
TVVR-18/5006
ISSN 1101-9824

Lund 2018
www.tvrl.lth.se

Master Thesis
Division of Water Resources Engineering
Department of Building & Environmental Technology
Lund University

English title:	Soil moisture modeling for agricultural needs in Brazil, France, and the U.S.A.
Author(s):	Filipe Fava
Supervisor:	Magnus Persson
Examiner:	Rolf Larsson
Language	English
Year:	2018
Keywords:	Soil moisture; HBV; Leaky-Bucket model; Thomson Reuters; NOAA

Acknowledgments

I am eternally grateful for all the support and education my parents provided me, who instructed me from a tender age on the high value of education for opening new doors.

I acknowledge the generosity and dignity of Sweden who, through its universities and other institutions present in our everyday lives in this country, offers life-changing opportunities for citizens all over the world.

I would also like to thank Thomson Reuters and its staff for proposing this thesis partnership, offering me continuous support and motivation from day one. Every single member of the Hydrological Research and forecast department (Stefan, Raza, Marion, and Markus) would always lend a helping hand and considerably improved the technical quality of this project.

Likewise, the academic support provided to me throughout the way was plenty and inspiring. Starting at my bachelor in the Federal University of Brasilia, the head of the Water Resources Department, Professor Sergio Koide, always captivated students with his expertise, seriousness and his life-long dedication to the student community and our society.

In Lund, from all the excellent professors within the department, Professor Magnus Larsson was individually responsible for most of the courses in our programme and always kept a friendly, exciting and proficient study environment. Regarding this specific project, Professor Magnus Persson played a crucial role in its development. He raised interest in this topic since the Rainfall-Runoff course lectures and was always receptive and resourceful in his supervision.

I could not forget about the friends I made on this journey. People with the most diverse backgrounds who cherished universally good values and made this a most pleasant ride. I am blessed to have had such a united, exciting group of classmates who, along with other members of the student and local communities, are engraved in my memories. A special thanks to Elizabeth Jenkins Sahlin, Jennifer Salvo and my brother, whom all have a special place in my heart.

Abstract

The purpose of this master's thesis project is to aid Thomson Reuters to forecast soil moisture, enhancing the agricultural productivity of its clients. This thesis focuses on testing the company's HBV model (HBV-TR) to accurately produce daily soil moisture values in Brazil, France, and the U.S.A.

The problem is that, up to this day, the most reliable monitoring of this soil water content is also through a model (the one-layer "Leaky-Bucket model"), whose results are only published as monthly hindcasts. This delay prevents most stakeholders from real-time information and planning.

By using input series similar to the Leaky-Bucket inputs, the HBV-TR simulated the target soil moisture for the last thirty-seven years. This project adapted the HBV-TR to calculate soil water with a one-layer and a three-layer version. The HBV-TR daily results are then compared to the monthly target series at consistent dates by the Nash-Sutcliff parameter, volume error, visual aspects, field capacity and evapotranspiration.

According to all these performance parameters, the results were sound, showing substantial evidence that this method can safely emulate the Leaky-Bucket model. Ultimately, this project concludes that soil moisture has potential to become the new feature in the company's forecast portfolio, providing planning capacity to more stakeholders.

Table of contents

List of Figures

List of Tables

Abbreviations

ha = hectare(s)
m = meters
mm = millimeter(s)
t = ton(s)

Acronyms

CAMS: Climate Anomaly Monitoring System
CDAS: Climate Data Assimilation System
CPC: Climate Prediction Center, an organ inside NOAA
GHCN v2: the Global Historical Climatology Network
HBV (model): Hydrologiska Byråns Vattenbalansavdelning, freely translating, Hydrologic Agency's Water Balance Section (model)
HBV-TR: Thomson Reuters' HBV
NASA: National Aeronautics and Space Administration
NCEP: National Center for Environment Prediction,
NSE: Nash-Sutcliff efficiency
NOAA: National Oceanic and Atmospheric Administration – U.S. Department of Commerce
UN: United Nations

U.S.A: United States of America
USDA: United States Department of Agriculture
USDC: United States Department of Commerce

1. Introduction

1.1 Background

The societal background of this thesis is the agricultural business and the food market and availability. According to recent UN's projections, world population is expected to increase to approximately 8.3 billion by 2030. Within this scenario, one of the primary goals in the 2030 Agenda for Development Goals is to eradicate hunger and achieve food security, which involves the promotion of sustainable agriculture and the implementation of practices that increase productivity and production (United Nations 2015).

Indeed, target 2.3 in that agenda is to duplicate the productivity and income amongst small-scale producers and family farmers through knowledge and increased investments in agricultural research (United Nations 2015). For great agricultural producers, target 2.4 addresses explicitly water quality and its sustainable use to correct food market barriers and distortions, avoiding extreme food price volatilities (United Nations 2015).

Given the present rising demand for food, maximizing the productivity in plantation fields is a common interest among producers, governments, and societies. Many programmes have been deploying remote sensing for soil moisture such as NASA, the United Nations, and for crop monitoring, such as the USDA and USDC through NOAA (Bolten, Crow, et al. 2010). This information, however, is only available nowadays to other stakeholders as monthly hindcasts (Huang, van den Dool, Huug M, et al. 1996), thus impairing the producers' water allocation capacity.

1.2 Objectives

To address this problem, Thomson Reuters has been looking into the possibility of forecasting soil moisture. To do so, it counts on its in-house HBV model in MatLab (HBV-TR), currently oriented for runoff calculations regarding energy markets. Considering that HBV-TR is a procedural model that calculates all water processes within a basin for local flow systems, Thomson Reuters wants to investigate whether HBV-TR can also produce accurate soil moisture values, similar to those produced by NOAA.

Beyond replicating, the purpose of this project is to model this soil water content in Thomson Reuters' way. NOAA, through its "Leaky-Bucket model," generates and publishes monthly hindcasts for soil moisture all over the global land surface having precipitation and temperature as an input. Thomson Reuters aims to use its HBV-TR along with similar input series to produce daily results consistent with these monthly targets. This project deploys the methodology above for regions in Brazil, France and the United States of America.

Well-established hydrological performance parameters assess the modeled series capacity to emulate the target series. According to the performance criteria here established, satisfactory results can signal the possibility for Thomson Reuters to forecast soil moisture, providing clients from agricultural businesses a tool for optimizing natural resources.

This project was divided into the following steps to reach its ultimate goal:

- introduce the theory behind water processes in the land surface and how different models approach these dynamics;
- describe the areas in which the model runs the simulations;
- inform about the collection, quality, and processing of the data;
- adapt, calibrate and validate the model;
- display and evaluate the results;
- conclude whether the HBV-TR can effectively model soil moisture.

1.3 Method

A literature review on soil hydrology and the models in view was carried, focusing on their routines and interactions between the independent variables. Additional research on local climate, topography, agriculture, and hydrology for the study regions of Mato Grosso, Picardy and Northwest Iowa provide a context for understanding the differences between the inputs and how they behave over time in these areas.

The next step displays the georeferenced input data for precipitation and temperature from NOAA, processed into tables. The data quality undergoes scrutiny regarding format, quantity, completeness, validity, and accuracy.

The missing values are filled in and graphically displayed for comparisons within and between regions.

Then, the HBV-TR model is set up to calculate soil moisture values. Two different structural arrangements are used to compute the water content in the soil for the regions above. The daily output series from this modeling is made compatible with the monthly target series, and the Nash Sutcliff efficiency, the volume error, NOAA's maximum field capacity, the evapotranspiration and the visual aspects are the selected parameters to evaluate the modeling performance. The calibration of the model parameters took place for the first thirty-three years, whereas validation would occur in the last four years.

Results are displayed and analyzed thoroughly for each of the performance parameters with the aid of graphs for both calibration and validation. The results are then discussed, basing the conclusion for this project, and pointing to further developments.

1.4 Limitations

This work abridges the correlations between meteorological data and soil moisture. The irrigation input to soil moisture is ignored, which in plantation fields is a primary contributor. The theory regarding evapotranspiration in the HBV-TR ignores central variables such as net radiation, wind speed, and plantation cover. Negative pressures within the unsaturated flow are also disregarded. Both HBV-TR and Leaky-Bucket abstract reality by overlooking such correlations.

The soil moisture target values from NOAA are already a product of modeling and not direct field measurements, containing the same assumptions as the HBV-TR. Furthermore, the Leaky-Bucket was only validated with gauged soil moisture and runoff values in small basins in Oklahoma, which does not attest its universal application (Huang, van den Dool, Huug M, et al., 1996). Therefore, this modeling does not aim to reproduce real measures, but also idealized ones.

Lastly, the areas put forth for modeling are whole regions or states englobing multiple basins. When considering the spatial heterogeneity of precipitation,

temperature, land cover, soil properties, and topography, one single averaged value does not characterize the many different soil moisture states throughout the area. Therefore, users of both target and modeled series must bear in mind the representativeness of these values.

1.4 Structure

After this introduction, the next section addresses the theoretical background involving soil moisture and the models by NOAA and Thomson Reuters. Chapter three depicts the investigated regions regarding their meteorology, economy, hydrography, and geography. The following chapter exposes the data as well as its collection, quality, and processing. Chapter five goes on to how to adapt, calibrate and validate the HBV-TR model for each of the three study areas. Section six displays the results, while chapter seven discusses them. Finally, chapter eight concludes and paves the way for further developments.

2. Theory background

2.1 Soil Hydrology components

Soil hydrology, or vadose zone hydrology, studies the physical interactions of water within the vadose zone as well as in its air and groundwater interfaces, including measurements and predictions of properties and processes (Shukla, 2011). These processes directly impact society by influencing agricultural production, environmental and water qualities, and the water distribution and storage on Earth (Shukla, 2011). Getting a grip of these dynamics enables sustainable practices and more access to natural resources.

The vadose zone, otherwise called unsaturated zone or aeration zone, is a three-phase system containing mineral grains and organic matter, water with dissolved solutes, and water vapor and other decomposition gases (Fetter, 2014). Soil surface, root zone, and transition zone can physically divide the unsaturated zone in three. The aeration zone is determinant to the sustenance of life on Earth, for it stores the water plants uptake. Beyond this, land use debris deposited on the soil surface might affect the infiltrating water quality, consequently contaminating rivers and aquifers (Shukla, 2011).

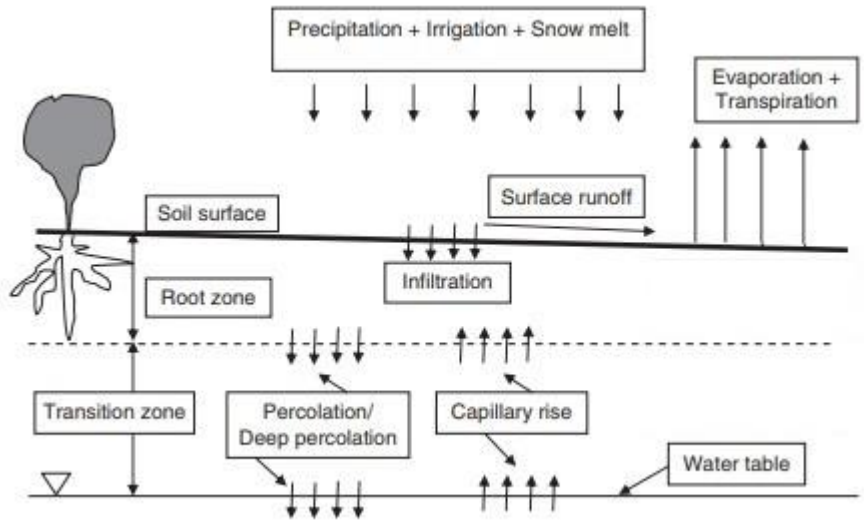

Figure 1: Water dynamics within the vadose zone (SHUKLA, 2011)

The core inputs of water occur at the air interface with the vadose zone. For precipitation to happen, a humid air mass must experience adiabatic expansion in an atmosphere filled with solid granular matter. Once the air mass cools until the dew point, droplets of water condensate around these nuclei, precipitating. If the forming raindrops are big enough not to evaporate until they reach the surface, rain falls on the ground (Fetter, 2014). When natural precipitation does not suffice for a specific culture, irrigation can aid that water supply.

It is also at the air interface where most water losses occur. According to works by Dunne & Leopold in 1978, plants can intercept as much as 35% of annual precipitation, eventually evaporating without ever reaching the soil (Fetter, 2014). Evaporation is a function of many variables such as latitude, temperature, water availability, radiation influx, solar hours of exposure and wind (Thornthwaite, 1948).

In land-dominated basins, plant transpiration is an even more significant contributor to water losses, for plants lose 99% of their water uptake through the micropores of their leaves in the form of water vapor (Fetter, 2014). Evaporation and transpiration are soil water losses impossible to separate in practice; therefore, evapotranspiration is the variable accounting for the total water vapor loss into the atmosphere (Thornthwaite, 1948).

When precipitation overcomes vegetation's storage capacity, water reaches the soil, being stored in ponds or infiltrating. Water infiltrates up to the specific infiltration capacity of a given soil, at decreasing rates over time as the vadose zone becomes more saturated until it reaches equilibrium (Fetter, 2014). Moreover, initial infiltration increases the amount of swelled colloidal particles in the soil, clogging waterways between voids, also reducing the infiltration capacity (Fetter, 2014).

Horton in 1933 and 1940 describes infiltration capacity in time according to

Figure 2 below:

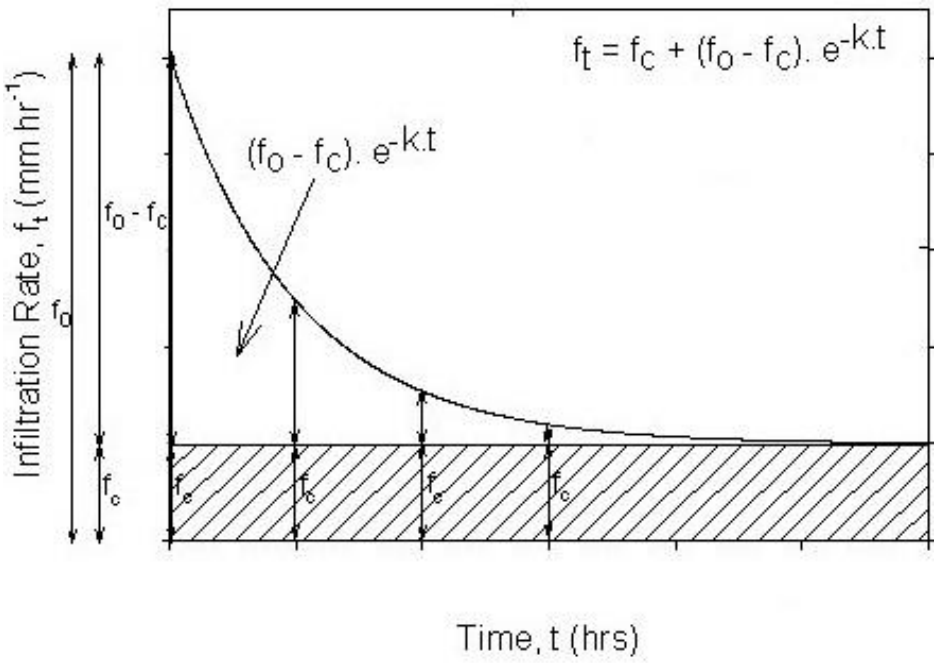

Figure 2: Horton's infiltration capacity curve, adapted from (Fetter, 2014)

where f_c and f_0 are the equilibrium and initial infiltration capacity, respectively, and K an experimental constant describing the decreased infiltration capacity (Fetter, 2014).

If the precipitation rate is higher than the infiltration capacity at a particular time, water will either accumulate in puddles to later infiltrate and evaporate, or flow overland according to the topography (Fetter, 2014). If soils are uniformly permeable, water will percolate vertically through the unsaturated zone until the water table, which at the same time outputs water into streams as baseflows (Fetter, 2014).

Depending on their size, lakes and reservoirs can be chief inputs to groundwater tables through direct precipitation (Bergström, 1992). The total surface runoff in a basin can also be composed by horizontal flow in the unsaturated zone -*interflows*- if the permeable unsaturated zone overlies on top of an impermeable layer (Fetter, 2014).

2.2.1 Soil moisture contents

According to the water inflows and outflows, the soil water content varies with time. Soil moisture represents the weight or volume rate of water and the soil media in the unsaturated zone. Considering saturation (S) to be the ratio between water and void volumes, while porosity (ϕ) the relation between empty and total volumes, soil moisture or volumetric water content (θ_v) can be expressed as a coefficient of the total volume according to Equation 1 below:

Equation 1 $$\boldsymbol{\theta_v = \frac{V_w}{V_t} = \frac{V_w}{V_v} * \frac{V_v}{V_t} = S * \phi}$$ (Tucci, Silveira, André L L da, 2009).

The capacity of plants to uptake water through the negative pressure in their roots can be a parameter to classify different components of soil moisture content. The water in the vadose zone available for nurturing plants is found in the belt of soil water, expending no more than 2 meters from the land surface (Fetter, 2014). When there is no more available water for plants – thus, reaching the *wilting point*- water is still present in the soil according to Figure 3 below.

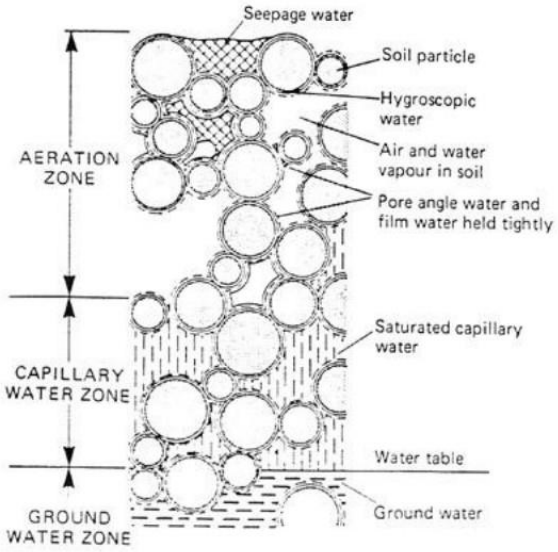

Figure 3: Soil water components below the wilting point (Larsson, R., 2017)

Capillary fringes arise due to negative pressures in fine-grained soils, also known as capillarity (Larsson, R., 2017)**.** Water might also be present in the aeration zone due to adsorptive forces, such as hygroscopic water and water vapor eventually enclosed between saturated voids (Larsson, R., 2017).

In a yearly cycle, the soil moisture seasonal variations can be extreme. In a hypothetical basin in a mountainous region, snowmelt and spring rain yield plenty of water on the land surface (Bergström 1992). During this period, the infiltrated water column in the soil might overcome the surface tension and recharge the groundwater table, characterizing this maximum water holding as field capacity (Fetter, 2014).

During long, dry summers, soil moisture content reaches its lowest levels due to high evapotranspiration, reaching close to the wilting point. After soil moisture recharge during the autumn, snowy winters with no infiltration leads the soil moisture content to drop asymptotically reaching the long-term field capacity. Indeed, gravity flow in the unsaturated zone might vary in time according to soil textures and compaction (Fetter, 2014).

Historically, soil holding properties have been recorded to characterize different soils (U.S. Department of Agriculture, 1955) as in Figure 4 below:

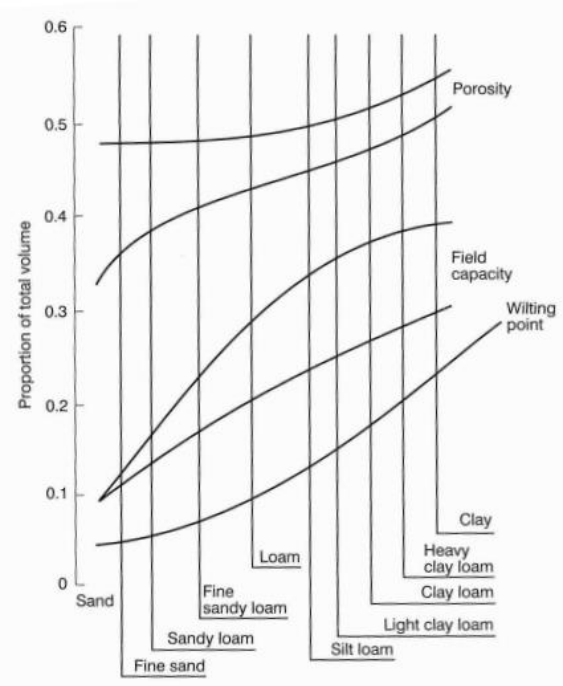

Figure 4: Water-holding properties of different soil textures according to Dunne et al. 1975 (Larsson, R., 2017)

Generally, the water holding properties increase proportionally to the surface area, inversely to the characteristic mean particle diameter considered. Thinner clay soils have a slightly higher void volume but are capable of withholding much more water than sand. In the other hand, plants can uptake water from sandy soils until lower limits in comparison to silt or clay.

2.1.2 Soil Moisture Flow

When infiltrating a dry land surface, gravity forces water downward through continuous void spaces while the soil matrix's negative pressures resist the flow (Fetter 2014). As water fills up the voids, the hydraulic conductivity by Darcy's law increases as matric suction decreases, for both are a function of the saturation conditions (Fetter, 2014).

Darcy's law applies when describing unsaturated flows (Fetter, 2014), in which water movement results from the product of hydraulic conductivity (K) and total potential according to the Equation 2 below:

Equation 2: $\boldsymbol{q = -K \times \frac{d\phi}{dz}}$.

The total potential ($\boldsymbol{\phi}$) results from opposing gravitational ($\boldsymbol{Z}$) and moisture potentials ($\boldsymbol{\psi}$). Moisture potential, or matric potential, or matric suction, is the same negative pressure that explains capillary fridges and is a function of the volumetric water content (Fetter 2014, Larsson, R. 2017). The total potential at a given depth in the unsaturated zone can be described by Equation 3:

Equation 3 $\boldsymbol{\phi = \psi(\theta_v) + Z}$

Richard combined the two equations above to describe the variation of soil moisture over time in the unsaturated zone as a function of hydraulic conductivity and matric suction according to the Equation 4 below:

Equation 4: $\boldsymbol{q = \frac{d\theta_v}{dt} = \frac{d}{dz}\left(-K \times \left(\frac{d\psi}{dz} + 1\right)\right)}$

The soil-specific three-way interdependency between soil water content, soil suction, and hydraulic conductivity can be seen in Figure 5 below:

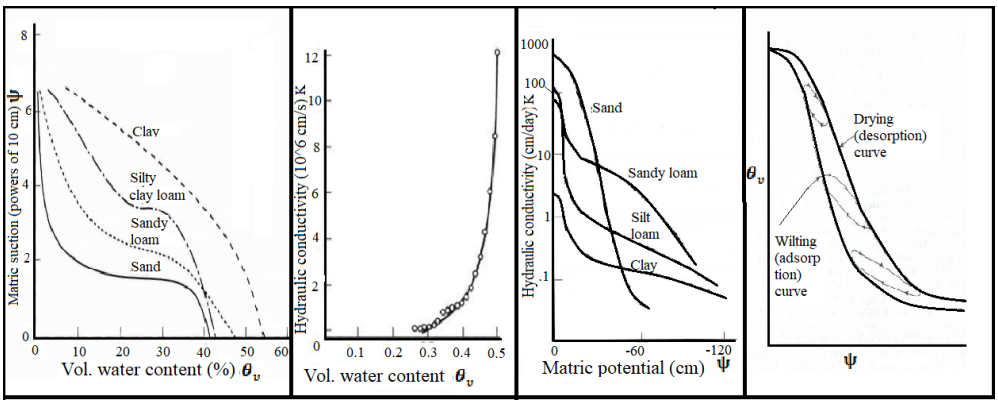

Figure 5: The relationship between soil water content, moisture pressure, and unsaturated hydraulic conductivity (Larsson, R., 2017)

The first graph of Figure 5 depicts the interdependency between volumetric water content and matric suction, registering over 10,000 meters of water column in drier conditions. Due to the larger surface areas, clays present more suction for any volumetric water content, up to 55% of water content.

The second graph in Figure 5 depicts the unsaturated hydraulic conductivity increase as a function of a wetter soil. The soil saturation can be deduced to be around 50% of water, where the hydraulic conductivity stabilizes. For the upper porosity curve from Figure 4, this second graph depicts light clay loam.

The third graph illustrates the combination of the two dependent variables. This graph shows that for low matric potentials, sandy soils have better hydraulic conductivity, whereas for dry soils sandy loams are less resistant to flow (Fetter, 2014).

Not only the pressures in unsaturated flow are functions of soil moisture; these pressures vary for a unique level depending on whether the soil is in a sorption or desorption cycle, according to the fourth graph in Figure 5. The behavioral change noticed is defined as hysteresis and complicates the unsaturated flow even more (Fetter, 2014).

There is a wide range of techniques to access soil hydrology parameters, usually focusing on soil moisture. Amongst field measurements are neutron probes, electric resistance and gamma-ray dampening measurers (Tucci, Silveira, André L L da, 2009). Many programmes deploy remote sensing for soil hydrology, which supplies information for a wide range of investigated fields, spanning from individual farming to regional and national scales (Bolten, Crow, et al., 2010).

Water availability and drought control are commonly calculated from mean absolute values of soil moisture content in millimeters, regardless of porosity of the vadose zone or its extent (Palmer, 1965). Absolute values are more accessible to all stakeholders, henceforth adopted in all next stages of this project.

2.2 CPC-NOAA Model

NOAA has created a drought information system to monitor soil moisture content. It deploys a so-called “Leaky-Bucket Model” for this task, a one-layer hydrological model based on the water balance of the vadose zone (NOAA, 2002). Precipitation and temperature are the only model inputs to estimate the water distribution between evapotranspiration, soil moisture,

groundwater loss, and runoff. The conceptual model can be seen in Figure 6 below:

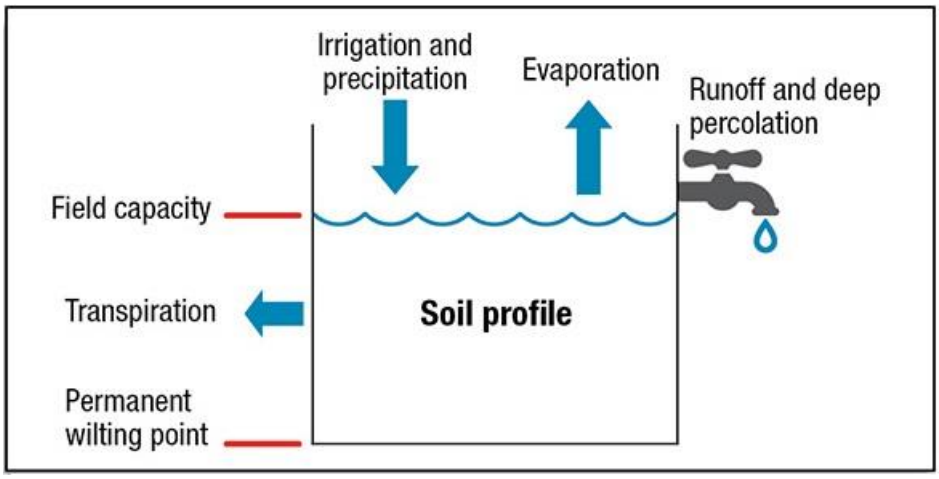

Figure 6: A conceptual Leaky-Bucket model (Yeik, 2014)

The model parameters were tuned based on Oklahoma observed surface flows and are constant in space (NOAA, 2002). The American agency deploys this routine monthly to hindcast soil moisture states on basins all over the world. In all its applications around the globe by NOAA, the maximum water holding capacity registered was 760 mm, which divided by a common porosity of 40% in volume indicates a total unsaturated zone of 1,6 meter (NOAA, 2002). Complying with this maximum field capacity is mandatory to validate the parameters and assumptions of new modelings.

One of these assumptions is that the water content involved in the calculations only regards the available water in the soil, ignoring all water content below the wilting point. Furthermore, the negative pressures involved in infiltration and unsaturated flow are assumed negligible, thus only considering the gravity in the potential differences. In the same line, hysteresis is also neglected, thus establishing a uniform behavior for any soil in both sorption and desorption cycles.

Variable unsaturated hydraulic conductivity is still valid, parameterized in function of the infiltrated water and the soil saturation state. Given the malleable definition of field capacity over time according to 2.2.1, here it is considered the total storage capacity of the soil, constant over time, validating

the model for any time-step. Whenever representing water contents, the variables regard absolute values in millimeters of water, abstracting surface dimensions, thus, homogenizing the results for the considered area.

Considering the model in its whole (Huang, van den Dool, Huug M et al., 1996), soil moisture can be estimated for a given area by Equation 5 below:

Equation 5: $$\frac{dW(t)}{dt} = P(t) - E(t) - R(t) - G(t)$$

in which W is the soil water content at time t; P(t) is the mean areal precipitation; E(t) is the mean areal evapotranspiration; R(t) the total runoff and G(t) the net groundwater loss through deep percolation.

The total runoff (R(t)) is composed of surface runoff - $P(t) * \left[\frac{W(t)}{FC}\right]^b$ - and base flow - $\frac{\alpha}{1+\mu} * W(t)$- parcels, respectively described by Equation 6 below:

Equation 6: $$R(t) = P(t) * \left[\frac{W(t)}{FC}\right]^b + \frac{\alpha}{1+\mu} * W(t) .$$

In Equation 6, in the first part determining the surface runoff, FC is the field capacity in millimeters, while $\left[\frac{W(t)}{FC}\right]^b$ is the parametrization for unsaturated hydraulic flow, where b is a free parameter with values greater than 1.

The second part of the equation determines the fraction that contributes to the base flow, where α is the inverse of the response time of the base flow, while μ is a dimensionless parameter that estimates how much of the subsurface flow will be turned into base flow in the drainage of the basin. The remaining parcel of Equation 5, G(t), represents unobserved groundwater flow, calculated according to Equation 7:

Equation 7: $$G(t) = \frac{\mu\alpha}{1+\mu} * W(t) .$$

Evaporation is given by Equation 8:

Equation 8: $$E(t) = E_p * \frac{W(t)}{FC}$$

In Equation 8, Ep is the potential value for evapotranspiration in a month, which in turn is estimated by the recorded temperature.

A well-established interaction between temperature and potential evapotranspiration is described by Equation 9 below, complemented by Equation 10 and Equation 11 (Thornthwaite, 1948):

Equation 9: $$E_p = \begin{cases} 0 & , \quad Ta < 0ºC \\ 16 * \left(\frac{L}{12}\right) * \left(\frac{N}{30}\right) * \left[\frac{10T_a}{I}\right]^{\alpha} & , \quad 0 < Ta < 26,5ºC \\ -415,85 + 32,25Ta - 0,43Ta^2 & , \quad Ta > 26,5ºC \end{cases} ;$$

Equation 10: $$\alpha = (6.75 * 10^{-7})I^3 - (7.71x10^{-5})I^2 + (1.792x10^{-2})I + 0,49239;$$

Equation 11: $$I = \sum_{i=1}^{12} \left(\frac{Tai}{5}\right)^{1,514} .$$

For the three equations above, *Ta* is the monthly mean surface temperature; *N* the number of days in the month calculated; *L* the average sunlight hours in the calculated month and *i* the ordinal number respective to the considered month (Huang, van den Dool, Huug M et al. 1996).

Potential evapotranspiration is estimated as a function of the observed temperature. Radiation influx is the most influent parameter for evaporation, and it is not a direct input to this model. However, by computing sunlight hours and temperature as parameters for net radiation, complex climatologic interactions can be objectively modeled (Palmer 1965)

2.3 Thomson Reuters Model (HBV-TR)

Thomson Reuters' in-house product is essentially a standard HBV model with outcomes focused on the electricity market in many different countries around the globe. The model assumptions for the unsaturated zone are the same as the Leaky-Bucket model in section 2.2. Darcy's law, Equation 2, is also valid for the saturated zone, driven only by gravitational potential.

Developed by the Swedish Meteorological and Hydrological Institute - SHMI- in 1972, the HBV model is the most widespread program for runoff modeling in the Nordic countries (Bergström 1992). In applications from lysimeter plots to the entire Baltic Sea drainage basin, its current version - *HBV96*- is in use in over 40 countries (SMHI 2015). HBV is suitable for

flood forecasting and spillway design flood simulations to water resources evaluation and nutrient load estimates (SMHI 2015).

Unlike the Leaky-Bucket, temperature and precipitation are the only input data for the HBV-TR, which respectively combine to a constant, *Tcorr*, or a coefficient, *SFCF* or *RFCF* as in Figure 7. Moreover, HBV-TR estimates potential evapotranspiration for every registered temperature combining it with a fixed constant, *Thorn*, specific to each basin. Ideally, an HBV model can be set to run at any desired resolution, depending on data availability (SMHI 2015).

The model is designed in a way to distribute the soil surface according to topographic elevations; in HBV-TR, seven sub-basins are present – according to the routines in the first box of Figure 7. This division allows for corrections in the climatological input according to patterns commonly observed in nature: the temperature lapse rate is usually -0.6ºC for each 100-meter increment in topography, as *TCALT* in Figure 7 (Bergström 1992). Likewise, precipitation also undergoes a distribution directly proportional to the altitude, *PCALT* in Figure 7, regulated in the model as a free parameter.

In its standard configuration, the model is structured in a series of four overlaying, sequential boxes, or routines, namely: Snow box, Soil moisture box, Upper Response/ Groundwater box and Lower Response/Deep Groundwater box (Bergström 1992), as shown in Figure 7 below:

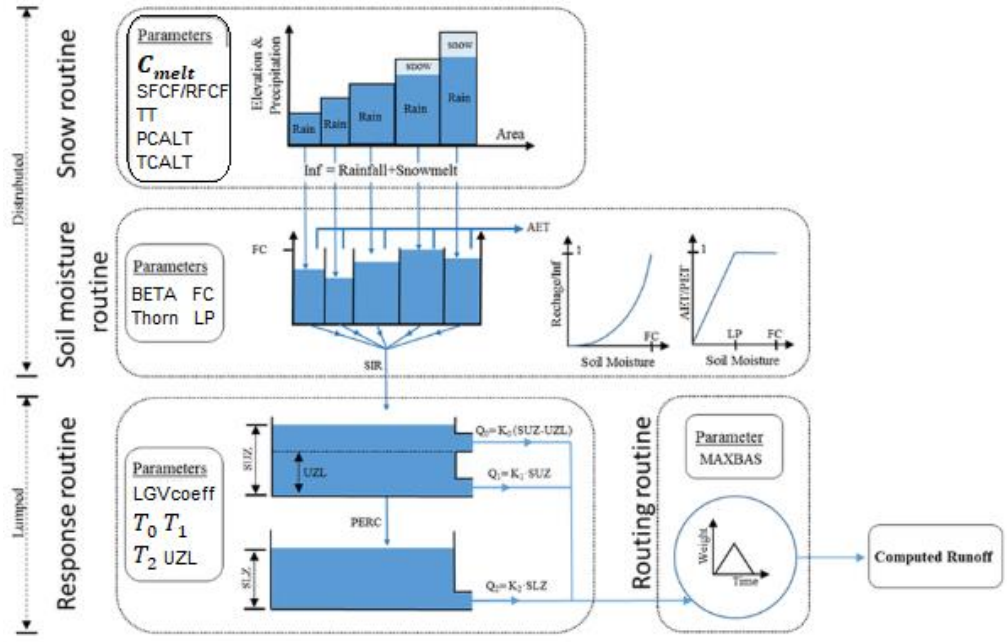

Figure 7: General HBV scheme (Jódar, Carpintero, et al., 2018)

Ideally comprising infinite horizontal dimensions in a daily time step, all parameters accounting for water and snow volumes in HBV-TR are vertical measurements in millimeters of water. The HBV-TR scheme can be described by Equation 12 to Equation 20 as follows.

2.3.1 Snow Box

The snow box deals with the snow accumulation and is the first distributed stage – as seen in the top box from Figure 7 (Jódar, Carpintero, et al. 2018). The threshold temperature, *TT*, defines whether precipitation occurs as snow or rain according to temperatures values below or above *TT*, respectively (SMHI 2015). In HBV-TR, *TT* is also the threshold over which accumulated snowpack starts melting according to the degree-day method explicated in Equation 12:

Equation 12: $$\boldsymbol{MELT(t) = C_{melt} * (T(t) - TT)}$$

In Equation 12 above, $MELT$ is given as millimeters of water at a given day t, while C_{melt} is a degree-day factor – a free parameter (cannot be physically measured but is inferred from calibration), that depends on the land cover,

given in mm/ºC*day -, *T* the daily average temperature in °C, and *TT* also a free parameter, in ºC. The snowpack in HBV is set to retain 10% of its mass in water, derived from both snowmelt and precipitation (Bergström 1992). The exceeding water from the snowpack input to the following box.

2.3.2 Soil Moisture Box

The soil moisture routine in the HBV model enables different storage capacities to each of the distributed sub-basins, resembling the Leaky-Bucket model as depicted in the second box in Figure 7 (SMHI 2015). This routine is where evaporation takes place, with four free parameters controlling all interactions, namely *FC*, *BETA*, *Thorn* and *LP* (Bergström 1992), according to Equation 13, Equation 14 and Equation 15.

Equation 13: $$\boldsymbol{EA(t)} = \begin{cases} \left(\frac{\boldsymbol{SM(t)}}{\boldsymbol{LP}}\right) * \boldsymbol{PE}; & \boldsymbol{SM(t)} < \boldsymbol{LP} \\ \boldsymbol{PE(t)}; & \boldsymbol{SM(t)} \geq \boldsymbol{LP} \end{cases}$$

in which the potential evapotranspiration is related to temperature by the *Thorn* factor as given by Equation 14:

Equation 14: $$\boldsymbol{PE(t)} = \boldsymbol{Thorn} * \boldsymbol{T(t)};$$

Equation 15: $$\boldsymbol{R(t)} = \boldsymbol{IN(t)} * \left[\frac{\boldsymbol{SM(t)}}{\boldsymbol{FC}}\right]^{\boldsymbol{BETA}}.$$

Soil moisture -*SM(t)*- at a given day follows a similar logic as in the bucket model – see Equation 5. Infiltration -*IN(t)*- is the input from the snow box (as P(t) in Equation 5), in the form of snowmelt from Equation 12 or precipitation as rain. In the other end, recharge -*R(t)*- is the output for surface runoff, identical to the first part of Equation 6 for the surface runoff.

The two graphs in Figure 7 depict the interactions between the variables in Equation 13 and Equation 15 in the soil moisture box. *LP* is the criteria for soil moisture content, given as a fraction of *FC*, the field capacity, below which evapotranspiration is a linear function of soil water content, as described in Equation 13 (SMHI 2015). *BETA* is a dimensionless parameter that regulates the increase in soil moisture storage for every millimeter of input from the snow box, parameterizing the varying unsaturated hydraulic

conductivity by Darcy`s law in Equation 2. Thus, the complement is the output to the runoff routine, as described in Equation 15 (SMHI 2015).

2.3.3 Response Routine

The averaged recharge from all sub-basins is the input to the runoff generation routine, composed of two lumped sequential boxes in the center-right of Figure 7. The upper box is a non-linear one, simulating quick, superficial channel discharges ("upper groundwater" in HBV-TR), described by Equation 16, Equation 17, and Equation 19. The lower one ("lower groundwater in HBV-TR") is responsible for base-flows in the hydrograph and responds linearly (SMHI 2015) according to Equation 20:

Equation 16: $\frac{dSUZ(t)}{dt} = R(t) - Qo(t) - Q_1(t) - PERC(t)$;

Equation 17: $Q_0(t) = (SUZ(t) - UZL) * T_1$;

Equation 18: $Q_1(t) = UZ(t) * T_0$

Equation 19: $PERC(t) = SUZ(t)/LGVcoeff$;

Equation 20: $Q_2(t) = SLZ(t) * T_2$.

SUZ(t) is the level of the upper groundwater box at a given time-step *t*. *UZL* is the threshold limit for the non-linear response, above which rules a recession coefficient (T_0) faster than the governing one at the bottom level (T_1). $Q_0 + Q_1$ is the total discharge from the upper ground water box, while *LGVcoeff* is the percolation coefficient to the lower groundwater box. Analogously, Q_2 accounts for the low groundwater discharge, expressed as a linear function of its water level *SLZ(t)*, considering a slower recession coefficient T_2. The lower box also accounts for the direct precipitation into rivers and lakes as well as their evaporations (SMHI 2015). The two models above have their main equations compiled in Table 1 below.

Model / Variable	LEAKY-BUCKET	HBV-TR
Evapotrasnpiration	$E(t) = E_p * \frac{W(t)}{FC}$	$EA(t) = \begin{cases} \left(\frac{SM(t)}{LP}\right) * PE; & SM(t) < LP \\ PE(t); & SM(t) \geq LP \end{cases}$
Potential Evapotranspiration	$E_p = \begin{cases} 0 & , \quad Ta < 0ºC \\ 16 * \left(\frac{L}{12}\right) * \left(\frac{N}{30}\right) * \left[\frac{10T_a}{I}\right]^{\alpha}, & 0 < Ta < 26,5ºC \\ -415,85 + 32,25Ta - 0,43Ta^2, & Ta > 26,5ºC \end{cases}$	$PE(t) = Thorn * T(t);$
GW Recharge	$G(t) = \frac{\mu\alpha}{1+\mu} * W(t)$	$R(t) = IN(t) * \left[\frac{SM(t)}{FC}\right]^{BETA}$
Total Runoff	$R(t) = P(t) * \left[\frac{W(t)}{FC}\right]^{b} + \frac{\alpha}{1+\mu} * W(t).$	$Q_0(t) = (SUZ(t) - UZL) * T_1$ $Q_1(t) = UZ(t) * T_0$ $Q_2(t) = SLZ(t) * T_2$

Table 1: Compiled main variables within soil hydrology for the HBV-TR and NOAA models.

3. Investigated areas

3.1 Mato Grosso, Brazil

Mato Grosso is a Brazilian State by the Bolivian border which spans over 900,000 km², depicted in Figure 8 (IBGE, 2017). It is mainly known for its exuberant forests, abundant water resources and for being an agricultural powerhouse (State Administration of Mato Grosso, 2015).

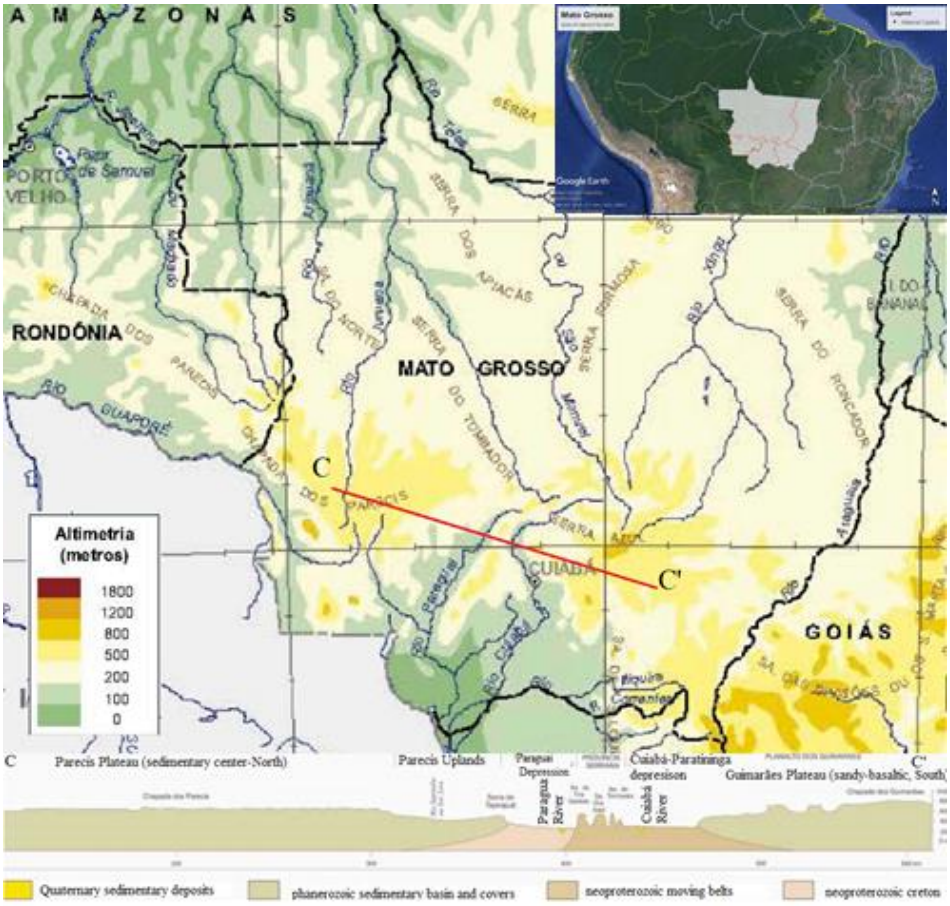

Figure 8: Location, topography and sectional cut in Mato Grosso, Brazil. Adapted from (Google Earth, 2017c, IBGE, 2010)

Mato Grosso is the third Brazilian State in size but only accounts for 1.59% of the population, with an estimated total count of 3.3 million inhabitants

(IBGE, 2017). The state name means *thick bush/forest*, and it is nationally unrivaled when it comes to biodiversity, being the only one in the federation with three biomes. The Amazon adds up to 53% of its territory while the Pantanal, the vastest flooded landscape in the world and Unesco's World Heritage and Biosphere Reserve, accounts for less than 10%. The other biome is the Cerrado, a markedly drier and more spread-out vegetation in flat planes, similar to the African Savannah (State Administration of Mato Grosso, 2015).

Mato Grosso is a state with low profile altitudes, characterized by broad, flattened surfaces throughout three distinct regions laying in sedimentary rocks mostly covered by red clay latosol, according to Figure 8. These are the sedimentary plateaus and crystalline uplands in the center-North, leveling at around 800 meters above sea level; the sandy-basaltic uplands and plateaus from the South; and the low lands from the Pantanal accounting for the Paraguay and Cuiabá-Paranatinga depressions around 200 meters above sea level (IBGE, 2010).

Regarding hydrology, Mato Grosso is one of the most abundant areas in potable water in the world, being the spring to the three most important river basins in the nation (State Administration of Mato Grosso, 2015). The Parecis plateau is the water divide between them, shown in Figure 8: the Tocantins, the Paraguay, which is a sub-basin to the Plata, and the Amazon (State Administration of Mato Grosso, 2015). A remarkable hydrology feature occurs in the Paraguay low lands, where due to mild declination and unconsolidated sediments on the margins, the river beds continually move, submerging large land extents on the depressions during the rainy season (EMBRAPA, 1982). This flooding enables the connection between the two most essential basins of the continent by boat, the Plata, and the Amazon, linking the east and west coasts (EMBRAPA, 1982).

The climate in Mato Grosso is mostly characterized as Tropical with summer showers (Souza, Mota et al., 2013). The estimated yearly average temperature is 29.7°C, with minimum and maximum averages of 22.8°C and 37.7°C, respectively (Barbarisi, Pilau et al., 2006). Locally, temperatures can vary widely: the capital, Cuiabá, seldom tops 40°C, while 60 kilometers south of it, negative temperatures have been registered at the Guimarães Plateau (State Administration of Mato Grosso, 2015). Yearly precipitations

can reach as much as 2,750 millimeters in the north of the state, being no lower than 1,500 millimeters elsewhere. Approximately 50% of the rain volume occurs during the summer months, in contrast to very dry winters with no more than 80 millimeters (Souza, Mota, et al., 2013).

The combination of warmth, profuse precipitations, and a vast, flat territory in a fertile land surface is one much favorable for agriculture. The State is seeded second in total agricultural production, a share worth US$13.5 billion, growing 10-fold over the past 20 years (IBGE, 2016). Mato Grosso is the leading annual producer for two of the top three most significant cultivations in Brazil: soybeans (27.3%) and corn (24%), which have alternated cycles around the year, usually sharing the same fields (IBGE, 2016). Mato Grosso has well-established agriculture, responsible for over 50% of the State yearly GDP, and is always in demand for new technologies to enhance its productivity (State Administration of Mato Grosso, 2015).

3. 2 Picardy, France

Formerly accounting for 19,400 km², Picardy is a historical territory and former administrative region of France, which englobed the *départments* of Oise, Somme, and Aisne. In 2016, it was merged with Nord-Pas-de-Calais *région* into *Hauts-de-France,* as part of a national reform to enhance bureaucratic efficiency (Encyclopædia Britannica, 2016). Figure 9 depicts the location below.

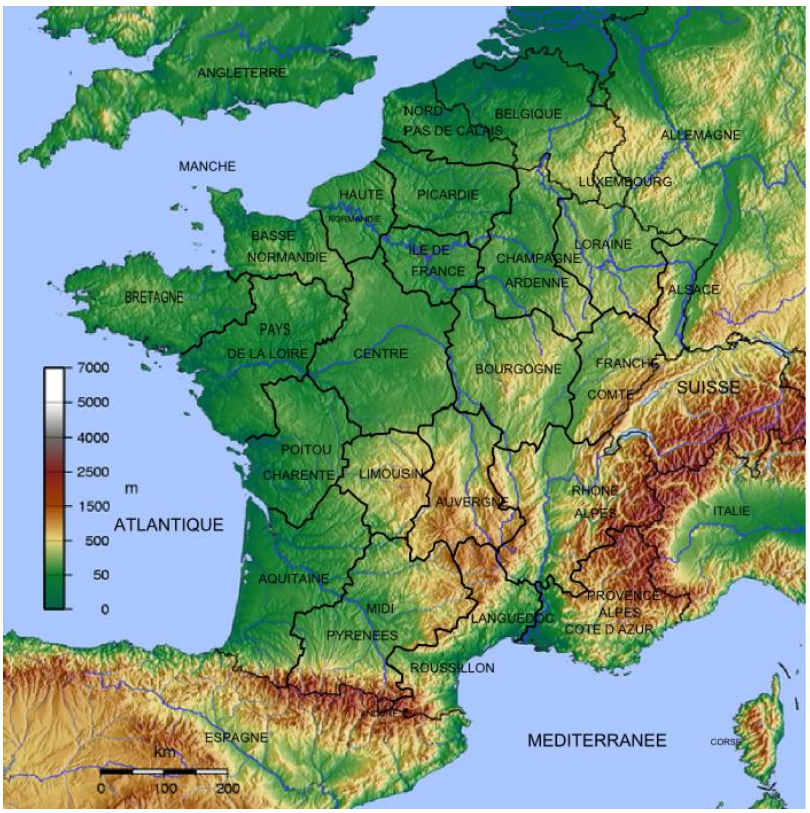

Figure 9: Location and topography of Picardy, France (Wikisoft, 2008)

Situated by the English channel north of the Isle de France, see Figure 9, Picardy is mostly drained by the Somme river, laying in a plateau of arable land within the Paris Basin (Schulzke, Kaule, 2001). Historically renowned for its strong agricultural productivity, Picardy's crops consist mainly of wheat (Encyclopaedia Britannica, 1820) and for the past decades, sugar beet (Oxford World Encyclopedia, 2004). Picardy currently ranks as the second region in France for wheat production, and its productivity of 8.4 t/ha is one of the highest in the world (Licker, Kucharik, et al., 2013).

The Paris basin consists mostly of plains and series of low plateaus interrupted by shallow valleys, with altitudes usually not higher than 200 meters (Embleton, 1984). The flat surfaces in Picardy are a result of early erosion in the basin, which lies on a broad chalk plateau (Blondel, Shennan et al., 2018). Clay-with-flints (loess) compose most of the local soil (Embleton, 1984), fertile for agriculture. When combined with its climatic conditions,

this set describes the most exceptional arable lands in the country (Blondel, Shennan, et al., 2018). The downside, however, is that virtually all woodland has been cleared by man since medieval times, interfering in the natural equilibrium (Embleton, 1984).

Picardy's climate is Temperate, for the most of it classified as Oceanic, but otherwise as Transitional Oceanic in its the eastern limits. Wet air masses coming from the Atlantic in a relatively abundant (ca 700 mm), well-distributed precipitation throughout the year characterize the Oceanic weather. Rains slightly peak between October and February and decrease in volume towards the countryside (Meteo France, 2017). Picardy averages annually 130 days of rain, accompanied by cloudiness, humidity, and haze (Meteo France, 2017).

Due to its northern location near the border to Belgium, winters in Picardy are colder than in other Oceanic climates in the country, with minimum mean temperatures around 1.5ºC during winter months, seldom going below zero (Meteo France 2017). In case it snows, it does not remain for long on the soil, due to the dynamic weather changes brought in from the Atlantic by continually blowing winds from the west (Blondel, Shennan, et al. 2018). During the summer, temperature averages around 18°C (Meteo France, 2017).

3. 3 Northwest Iowa, U.S.A.

Iowa is situated in the Continental United States, bordering the Mississippi River on the East side and the Missouri River and the Big Sioux River on the West, as seen in Figure 10. As a part of the Corn Belt, Iowa has always played a pivot role in the American economy as a rural state, with over 90% of its area designated to agriculture. Nonetheless, this business employs less than 10% of the workforce in the state, which has been diversified since the turn of the millennium (Encyclopædia Britannica, 2018). Iowa's main agricultural products are corn, soybeans, hogs, and cattle; its production is mostly exported, sent by rail and truck to Mississippi River, allocated, then, in barges for shipment to the Gulf of Mexico (Encyclopædia Britannica, 2018).

Figure 10: Location, topography, and rivers in Northwest Iowa, U.S.A. Adaptation from (Maps of the World, 2017)

The investigated area, shown by the black line in Figure 10, adds up to approximately 14,000 km² or nearly 10% of Iowa. It consists mainly of the Northwest Plains, the highest lands in the state. Topography is described as a "gently rolling landscape" with a well-fixed network of streams across the entire region (Prior, Iowa 1976), accounting for most of the lakes in the state (NOAA, 2018). Northwest Iowa is a transitional landscape to the high planes of the Dakotas, with a remarkable decrease of native woodlands when compared to the rest of the state (Prior, Iowa, 1976).

The topography in from the Northwest Plains also influences precipitation. Pluviometry in the area registers mean records below 625 millimeters annually, around 25% lower when compared to more abundant regions in the State, (Prior, Iowa 1976). Rainfall is unevenly distributed throughout the year, heavily concentrated in the summer (Encyclopædia Britannica, 2018), when the dominant moist air flow from the Gulf of Mexico produces a maximum (NOAA, 2018). During the winter months, the Canadian air flow creates a considerably cold and dry climate (NOAA, 2018). Therefore, the

investigated site is the most elevated, driest and less forested in the whole state.

Iowa presents a well-divided four season-climate, as most areas deep into that continental land. In January, the coldest month of the season, temperature averages -15°C early in the mornings and -5°C in the afternoons (NOAA, 2018). However, snowfall (32 inches on average) is comparatively low considering the neighboring states (Encyclopædia Britannica, 2018), rarely remaining throughout the whole winter. Nonetheless, substantial snowfalls on the beginning of the spring followed by rapidly increasing temperatures and strong showers have left the state severely flooded for months on different occasions, such as 1993 and 2008 (Encyclopædia Britannica, 2018). Temperature surpasses 32ºC, on average, between 8 days -Northeast- and 36 days -Southwest of state (NOAA, 2018).

The state of Iowa is prone to several natural hazards. Around 85% of the thunderstorms (55/year) that hit the State occur between April and September, producing hail, strong wind currents, torrential rains and occasionally tornadoes (46/year) at the peak season, in June (NOAA, 2018). Tornado occurrences prevail between May and June, usually spread over 16 days. Hailing occurs only between two and four days per year but are responsible for crop losses around 1.4-4.5% depending on the culture, and are even more severe in the Northwest Plains (NOAA, 2018). Droughts frequently occur, historically damaging the local economy more than all other weather events combined (NOAA 2018).

Its soil is mainly configurated by loess at the surface, topping a clayey glacial till, occasionally forming springs and seeps. These phenomena result from groundwater standing on impermeable till layer until reaching acutely-sloped topography (Prior, Iowa 1976). As with most of Iowa, the terrain is well suited to the cultivation of crops, dark in color and rich in organic matters and minerals (Encyclopædia Britannica, 2018). However, the typically low soil moisture of the region, coupled with hot, dry winds in autumnal “Indian Summers,” demand extra attention regarding the conservation and efficiency of water use to secure the harvest (Prior, Iowa, 1976, NOAA, 2018).

Table 2 presents a summary of the regional descriptions below.

Area	Precipitation	Temperature	Natural Hazards	Soil / Topography	Rivers / Watersheds	Economy
Mato Grosso	*1500-2750mm *Wet and dry seasons	* mín, mean, max daily T: 22.8°C; 29.7°C; 37.7°C * ≠ local Ts	*Floods *Moving river beds	*Eroded, mostly clay latosol * Mostly Plateaus 800 m a.s.l.	*Cuiabá and Paraguai rivers *Tocantins, Plata and Amazon	*Soy *Corn
Picardy	*+- 700 mm *Well distributed * little snow accum.	*season mín and max avg.: 1,5°C ; +18°C *Quick weather	-	*Eroded, clay w/ flints *Low, flat surfaces 200 m a.s.l.	*Somme *Mostly in Paris basin	*Wheat *Sugar beet
NW Iowa	*>625 mm *Wet and dry seasons *snowpack most of the winter	*daily mín and max avg.: -15°C ; +32°C *Quick weather changes	*Thunderstorms *Hails *Tornadoes *Droughts	*Dark loess, rich in organic matter and minerals *Plains ca 500 m a.s.l.	*Sioux and Misouri rivers	*Soy *Corn

Table 2: Local features summary for Mato Grosso, Picardy, and Northwest Iowa

4. Data

4.1 Collection

The precipitation input herein onward adopted is from CPC's PRECipitation REConstruction over Land project. This analysis consists of reconstructed records using GHCN v.2 dataset, interpolated for over 17,000 gauge observations over land, along with anomalies dataset registered in CAMS (Chen, Xie, et al. 2002). In this series, the precipitation climatology is analyzed separately from the anomalies series, added up together afterward to generate the total precipitation (Fan, van den Dool 2004).

The temperature series selected is from the Climate Forecast System Reanalysis (CFSR), which was performed by NOAA's NCEP (Saha, Moorthi, et al. 2010). CFSR is a modeled data which deploys satellite observations, accounting for variations in the levels of carbon dioxide, aerosols, trace gases as well as solar variations (Saha, Moorthi, et al. 2010).

The soil moisture target values are calculated from monthly time series of accumulated precipitation and mean temperature by the Leaky-Bucket model (as described in 2.2) with spatially-constant parameters (Huang, van den Dool, Huug M et al. 1996, Huug van den Dool, Jin Huang, et al. 2003). It represents the soil condition on the first day of every month, after the action of a whole month of climate input. NOAA used CPC's PRECipitation REConstruction over Land as the rainfall input data, while the temperature series is NCEP`s Reanalysis/CDAS v.2 or CDAS2 two-meter air temperature (Huug van den Dool, Jin Huang, et al. 2003)**.**

Thomson Reuters' Agriculture Department provided the study areas through internal communication, where potential clients could benefit from the implementation of this new forecast.

4.2 Quality of data

A product of a modeling can only be as good as the quality of its input data. The areas selected by Thomson Reuters are the georeferenced polygons on Google Earth files depicted in Chapter 3. Both climatological input and soil moisture data are georeferenced to the same 0.5º x 0.5º grid over the globe

from February 1st, 1981 to December 1st, 2018. Precipitation, soil moisture, and temperature have a daily resolution and are available in millimeters and degrees Celsius, respectively.

The precipitation records are directly obtained from the field with a four-digit significance, registering 1780 missing values in the Brazilian region (4,17days/37 years); in France, 920 values were missing, or 27,9 days/37 years; while in the U.S.A., only 404 flaws, or 4 days. The series from each cell are direct measurements, averaged from observation stations. The more functioning observation stations influencing the values of a grid cell, the higher the gauge density of that cell. Grid cells with the same number of contributing observation stations might have different gauge densities if in one of them the observations are constantly interrupted by technical problems, for example. Some grid cells might not even encompass any gauged data at all, interpolating their data from neighboring cells. The colors in Figure 11 depict the gauged density of observed values for precipitation in excluding intervals as portrayed below.

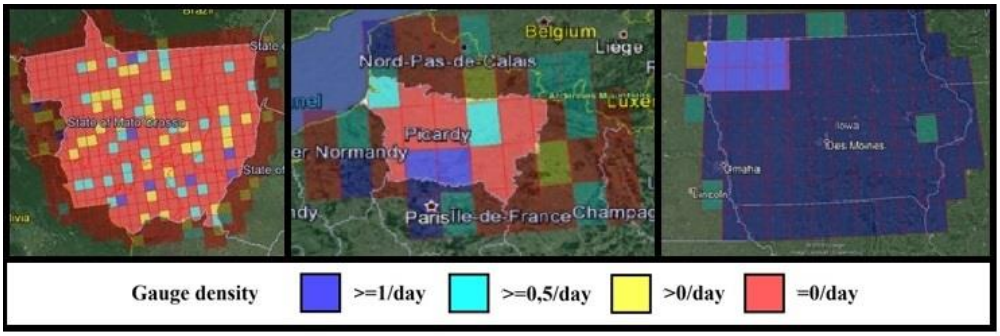

Figure 11: Precipitation gauge density over the grid for all three areas(Google Earth 2017a, Google Earth 2017b, Google Earth 2017c, Thomson Reuters 2018)

The CSFR data is obtained indirectly, once the temperature themselves were not measured, but estimated by correlation with radiation from the land surface, captured by satellite. This temperature data is available at 64 vertical layers in the atmosphere, in an hourly resolution, also with a four-digit significance (Saha, Moorthi et al. 2010). If no technical problems occur, every cell in the grid will have their temperature recorded from one satellite scan; hence, gauge density does not apply. When analyzing completeness, the temperature series is very satisfying. In Brazil, amongst all pixels, there are

only 25 unfilled values, representing a failure equivalent to 1/9 of a day in the whole series. In France and U.S.A., there is no missing data at all.

The modeled soil moisture data reported by NOAA monthly is initially available in the grid format as the input series, which is to say there is one Leaky-Bucket model per cell. Before reporting these values, NOAA fills in its missing input data, so the soil moisture series is entirely complete. While the precipitation input series used is the same for NOAA and the modeling carried in this project, the temperature series are slightly different.

NOAA deploys the NCEP CDAS series, which uses some technology and algorithms that have become inadequate over time. An example is the initial atmospheric conditions conceived in the 1990's coupled with model components from a decade later (Saha, Moorthi, et al. 2010). Despite CDAS being one of the most used NCEP products in history, the NCEP CSFR series show a far better time and space resolution, greater covered area, better data assimilation system and forecast model (Saha, Moorthi, et al. 2010). The NCEP CFSR deployed in this project will provide the basis for most of NCEP's climate products and forecasts in the forthcoming years(Saha, Moorthi, et al. 2010).

4.3 Data processing

The georeferenced precipitation and temperature series were processed by Thomson Reuters's agriculture and climate department and transformed into a table in text extension. Each cell from the 0.5° x 0.5° grid was assigned a column and a name symbolizing its geographic location, and the registered values for each cell displayed in chronological order. Thus, one table for each climatological input was created encompassing all three regions.

The gridded georeferenced soil moisture series, however, had to be expressed as one single value per region, enabling comparison with the single results from the HBV-TR, as described in 2.3. The gridded cells had their monthly values averaged, thus yielding a one column table for each region. The only cells used to calculate the unique regional soil moisture are the ones contained inside the study areas, represented in Figure 11. Logically, these were also the cells pre-selected for the input series. Thomson Reuters mined

the values for surface temperatures (2m) and compiled the data in a daily-average format (Thomson Reuters 2018).

The input data was completed to yield flawless soil moisture results. The missing values for precipitation were assumed to be zero, considering their low occurrence do not affect the yearly water budget. Given the small range of variation in temperature in Mato Grosso, the series average replaced the unregistered figures. The soil moisture target data did not require any treatment in that sense.

The processed metadata from the gridded cells and the soil moisture series were plotted over time to verify the validity within and between data sets. Illustrations of daily input data from two distant gridded cells in each region were compiled monthly, further aided by monthly and yearly statistics, as seen in the auxiliary graphs in Figure 12, Figure 13, Figure 14 below.

Figure 12 is mostly consistent with the depiction of Mato Grosso in Chapter 3. Temperatures are close to 25°C all year round in the first auxiliary graph, slightly below the 27.8°C mean from 3.1, with a pronounced rain period during summer months. Considering Mato Grosso's vast territory, gauged values do vary significantly, averaging from 1500 mm to over 2400 mm of precipitation. Temperature also behaves distinctly, as is depicted in the first auxiliary graph, with winter records up to 13% lower.

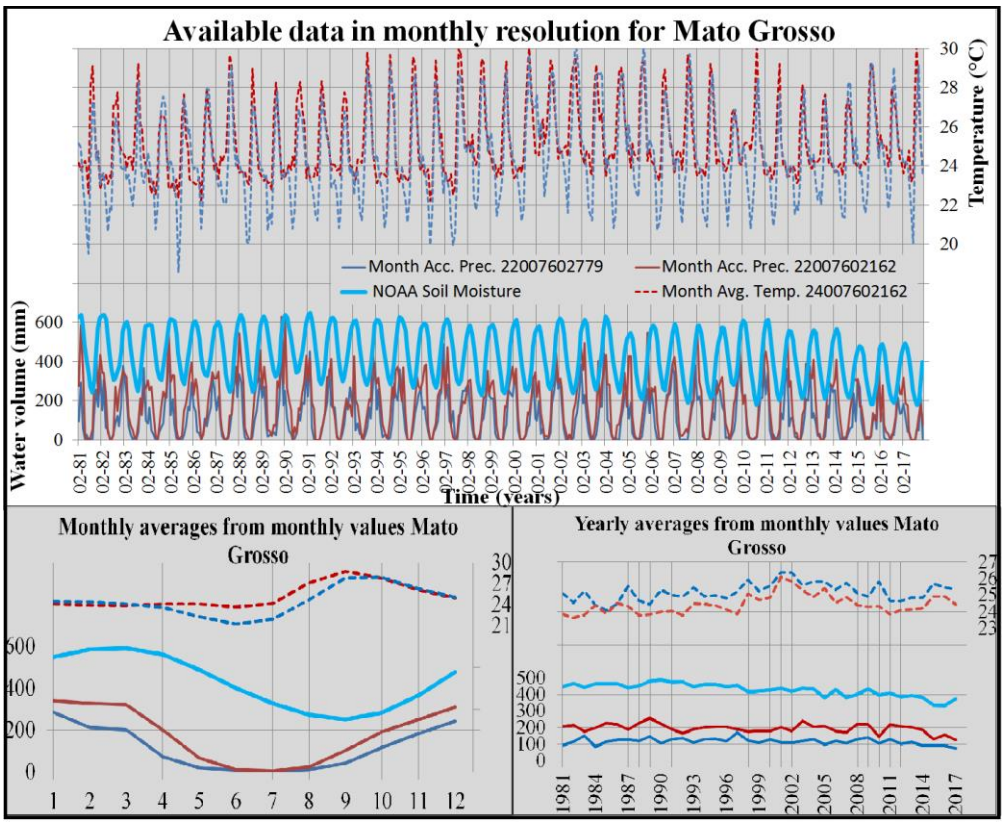

Figure 12: Processed input data for Mato Grosso

Figure 12 also shows an interestingly steadily varying cycle of soil moisture. According to the monthly averages from monthly values graph, soil moisture values increase during the first months of the year, when water is abundant. When winter arrives, and precipitation ceases, soil moisture drops while temperatures rise from July to September, creating the driest periods in the soil. Rains timidly start again in August, and by October the soil moisture is already on the rise.

Figure 13 below is according to the general description of Picardy given in Chapter 3. In a temperate climate by the ocean, the area presents monthly mean minimum temperatures slightly above 0°C and mild summers around 17°C, as in 3.2. It is also interesting to observe that grid cell number 0087 is colder during the winter, according to the monthly averages from monthly

values graph. That can be attributed to its location far into the continent, whereas cell 0075 by the coast is thermally better isolated.

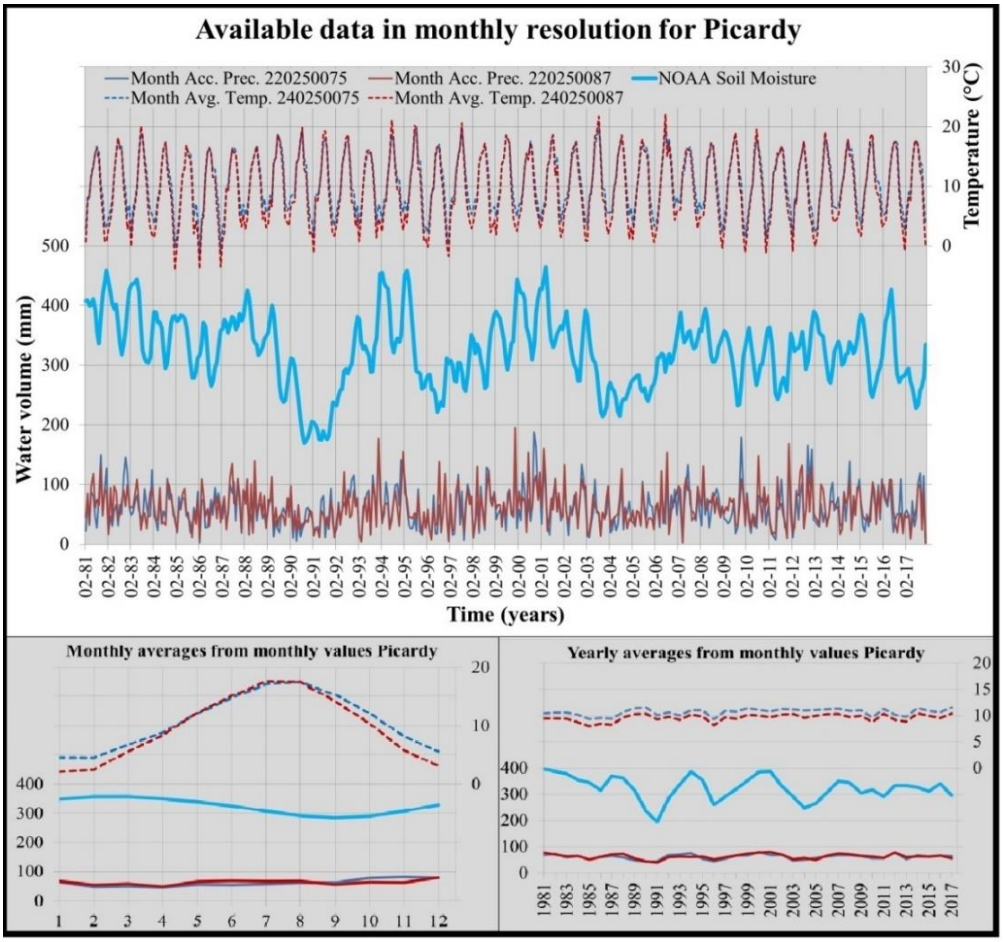

Figure 13: Processed input data for Picardy

Figure 13 shows a well-distributed rainfall over the year averaging 800 mm yearly according to the first auxiliary graph, slightly superior to the 700 mm average from section 3.2. The "monthly averages from the monthly values" aid graph illustrates a clear correlation between temperature and soil moisture. The yearly averages aid graph, on the other hand, makes the dependency between soil moisture and precipitation explicit, when it aligns points of maximums and minimums from both series.

Figure 14 below portraits the Northwest region of Iowa in resonance with the description from Chapter 3. A Continental climate, with distinct seasons around the year, with mean monthly temperatures ranging around -10°C to nearly +24°C, seen in the first auxiliary graph. This variation is representative to the description in 3.3, where daily extremes of -15°C and +32°C occur. Rain records are slightly higher than in the description, averaging 700 mm yearly, concentrated around midsummer. Grid cell number 3193 presents slightly lower precipitations for being the most northwestward for Iowa, while 3297 is in the opposite location.

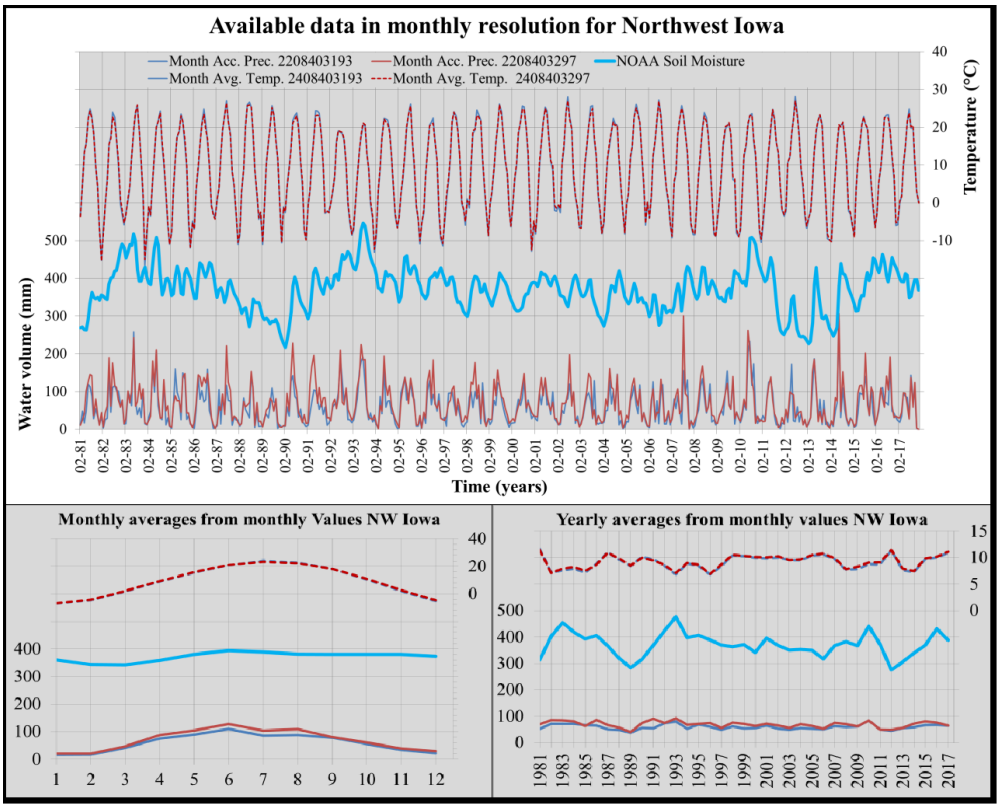

Figure 14: Processed input data for Iowa

The monthly averages from Figure 14 show that soil moisture decreases during winter despite the absence of evaporation considered in those temperatures. In the same Figure 14, the "yearly averages from monthly values" graph displays both influences of precipitation and temperature in soil moisture values, with rainfall being a more predominant factor.

5. Modeling soil moisture in HBV-TR

5.1 Model adaptation

Considering the HBV-TR original runoff orientation, its daily time-step capacity and calculations for all the variables described from Equation 12 to Equation 20 in table format, the first adjustment needed is to display the results for soil water content instead of runoff.

An adaptation for the HBV-TR model would be to consider only the water content from the soil box described in subsection 2.3.2. This adjustment transforms the HBV-TR into a one-layer model, physically similar to the Leaky-Bucket from NOAA in section 2.2. Evapotranspiration in both models is a function of the soil saturation and temperature, see equations 8 and 13. Likewise, both models assume water losses dependent on the saturation level according to equations 6 and 15. This version for soil moisture calculation modeled the Brazilian basin.

However, this HBV set-up has a limitation when emulating long-term field capacities during winter, as described in subsection 2.1.1 and visible from Figure 14. According to Equation 15, this box never loses water in negative temperatures, for there is no evapotranspiration nor infiltration from snow to force groundwater recharge. If many consecutive days register low temperatures, as is the case for Iowa, then the soil moisture values would remain constant for months.

To account for gravitational losses like the Leaky-Bucket, the second configuration for the HBV-TR was to include the response routines, which act according to Darcy's law in Equation 2. This second HBV-TR set-up modeled the Picardy and Iowa regions.

5.2 Computing model performance

The performance analysis of a hydrologic model demands objective and subjective estimates to enable a reliable conclusion (Krause, Boyle, et al. 2005). The most important approach to evaluate modeling performances is through the visual assessment of systematic (over or underestimations) and dynamic aspects, such as timing, baseflow, rising and falling limbs (Krause,

Boyle et al. 2005). Nonetheless, for quantitative evaluations, efficiency criteria must be coupled with a volume error assessment (Krause, Boyle, et al. 2005).

A frequently used performance criterium for runoff models in literature is the Nash-Sutcliffe (NSE) (Krause, Boyle, et al. 2005), which can be described by Equation 21:

Equation 21: $\boldsymbol{R^2 = 1 - \frac{\sum_{t=1}^{T}(SM_m^t - SM_o^t)^2}{\sum_{t=1}^{T}(SM_o^t - \overline{SM_o})^2}}$, for which $\mathbf{SM_m^t}$ stands for the modelled soil moisture in a time step t, whereas $\mathbf{SM_o^t}$ is the observed target value for the same period, and $\mathbf{\overline{SM_o}}$ the average of the observed series. The NSE coefficient equals one when the modelled and observed series are identical; a value of zero indicates that the modelled series is as good as the simple mean of the observed values (Moriasi, Arnold et al. 2007). For this thesis, the, acceptable threshold has been stipulated as 0.8 (Thomson Reuters 2018).

Another criterium commonly resorted to when assessing runoff models is the relative volume error. It describes the general tendency to estimate the observed series, expressed as follows in Equation 22:

Equation 22: $\boldsymbol{\mathrm{Vol.\,error} = \frac{\sum_{t=1}^{T}(SM_m^t - SM_o^t)}{\sum_{t=1}^{T}(SM_o^t)} \times 100\%}$.

In implementing the concept of volume error from runoff to soil moisture content, it is intuitive that it will constitute an accumulated volume error. Accumulated volume differences will inevitably occur, but the desired volume variation should be within 10% (Thomson Reuters 2018). Henceforth, accumulated volume error will be basically referred as "volume error", given its widespread usage, immediately conveying the right concept to the reader.

A relative criterium to which this project will also implement is the evaporation rates from the modelings. Evaporation rate is the percentile relation between the total amount evaporated compared to the total precipitation. This rate can vary widely but allows comparisons between basins' performances. In the same line, the maximum water holding capacity for each region will be accessed and compared to NOAA's threshold of 760 millimeters, according to section 2.2.

The comparison between the evapotranspiration series from both models will also add to the validation of the methodology deployed. This way, the water output to the atmosphere will compare whether both models can describe the basin similarly, not only the target values. This validation can indicate improvements in the calibration or the approach taken if by-product series are distinct.

Difficulties arise when computing performance in the HBV-TR: soil moisture will be modeled daily, while the target series is in a monthly resolution. It is only rational to compare data series with the same length and resolution, as noticed from Equation 21 and Equation 22. Trying to force a higher resolution in the monthly series is not feasible, for any mathematical distribution of the monthly variations into days would nullify the direct relation between daily observed weather and soil moisture, a relation which is the very core of this work.

The alternative, however, seems more reasonable. A monthly series cherry-picked from the daily modeled values can be compared to monthly target soil moistures at the same dates, thus proving the daily modeling capacity. This way, both series consider a monthly variation between soil moisture conditions after climate action, the HBV-TR soil moisture being an accumulated result of daily mutations.

5.3 Calibration

The time length of the available data is split between the calibration and validation phases. To have them simulated independently emphasize the parameter tuning from calibration. The time division herein on adopted aims to prove the model accuracy in both short and long periods. The calibration assigned spans from February 1st, 1981 until October 1st, 2013, while the validation occurs in the last four years, between October 1^{st,} 2013 to December 1st, 2017.

It is unknown how NOAA calibrated every single Leaky bucket on the 0.5° x 0.5° cell grid. Therefore, it is necessary to calibrate the daily gridded records to achieve the best input combination for this modeling. Given that this process is done manually, weighing more than 8-10 cells become unpractical, requiring some previous selection.

Considering the grid layout over the studied areas in Figure 11, only grid cells that overlap those areas are relevant. Due to Mato Grosso's vast dimensions, the next selection criterium adopted was the gauged density. Denser gauged cells (blue, green and yellow, in that order) are more representative than those cells which only interpolate from neighboring cells (red), as seen in Figure 11. Grid cells far from each other are more likely to express distinct patterns, while neighboring grid cells can be redundant, especially for temperature, given its space-time continuity (Yun Fan, Huug van den Dool 2008).

Fixing standard HBV-TR model parameters, the performance coefficients in Equation 21 and Equation 22 can evaluate initial simulations through sensitivity analysis, followed by an iterative calibration leading to the final weighing as presented in Table 3 below.

NORTHWEST IOWA - USA				MATO GROSSO - BRAZIL				PICARDY - FRANCE			
P-Station	1,00	T-Station	1,00	P-Station	1,00	T-Station	1,00	P-Station	0,00	T-Station	1,00
2208403194	0,10	2408403194	0,05	22007602162	0,05	24007602162	0,05	2202500096	0,01	2402500096	0,08
2208403193	0,05	2408403193	0,05	22007602231	0,55	24007602231	0,75	2202500097	0,01	2402500097	0,58
2208403195	0,10	2408403195	0,05	22007602165	0,05	24007602165	0,05	2202500075	0,01	2402500075	0,08
2208403196	0,40	2408403196	0,05	22007602295	0,35	24007602295	0,15	2202500085	0,02	2402500085	0,03
2208403297	0,10	2408403297	0,05					2202500083	0,80	2402500083	0,06
2208403296	0,10	2408403296	0,70					2202500084	0,14	2402500084	0,06
2208403295	0,10	2408403295	0,05					2202500086	0,01	2402500086	0,06
2208403294	0,05	2408403294	0,00					2202500098	0,01	2402500098	0,07

Table 3: Weight distribution for gridded input series

The weighed values attributed to each gridded cell are in every second column, adding up to 1, the total contribution. While in the smaller regions all gridded cells were considered to substantiate the moisture product, the selection in Brazil narrowed the input of gridded cells to four. Spread grid cells from the three different regions described in section 3.1 Mato Grosso were enough to represent the typical behaviors in the state.

With an optimized weight distribution for input data, the free parameters from the HBV-TR model are set to undergo calibration. After manual sensitivity analysis for each of the parameters, the best set found for each study area is as follows in Table 4.

AREA	Tcorr (°C)	sfcf	rfcf	TT (°C)	MELT (mm/°C *day)	Thorn (mm/°C)	hp	fc (mm)	b	LGV coeff	UZL (mm)	T0	T1	T2
IOWA	1,3	0,85	1,0	-2,0	7,0	0,122	0,9	430	2,15	80	∞	15	32	140
PICARDY	2,0	1,00	1,0	0,0	4,0	0,172	0,95	530	1,30	80	∞	15	28	120
MATO GROSSO	1,8	1,00	1,0	0,0	4,0	0,180	0,98	630	3,00	50	-	-	-	-

Table 4: Parameter calibration for HBV-TR

HBV-TR allows for a correction factor in temperature and coefficients for the input precipitation, as seen in Figure 7 and section 2.3. The temperatures were increased between 1.3 to 2°C for all records. *Thorn* is the coefficient that relates temperature to potential evapotranspiration, according to Equation 14. *LGV* is the recession coefficient that regulates the water transfer from upper to lower groundwater boxes according to Equation 19. Most parameter sets from this calibration are consistent with expected values for their respective field according to Thomson Reuters' experience. However, the values for *Thorn* for Brazil and France are higher than the usual 0,15 upper limit (Thomson Reuters 2018).

6. Results

6.1 General remarks

The results here presented base the deployment of the performance criteria both objectively and subjectively, according to section 5.2. While the objective criteria are straight-forward and as simple as a three-digit number, it is commonly the visual aspect which enables a thorough understanding of the modeling and indicates further developments, as seen in the following sections.

Because of the negative temperatures and the model adaptation implemented, as explained in Chapter 5, many more variables compose the soil moisture content in the regions of Picardy and Northwest Iowa in the following graphs. Their secondary vertical axis now includes snowmelt in small quantities, serving the ultimate purpose of a holistic visualization of the variables in play. Some liberties were taken from conventional methods for presenting the values in a logical, clear way.

The secondary vertical axis is dimensionless and shows the climatic variables. These are plotted in the superior part of the graph in an inverted scale (except Figure 15), as to represent their disposition in nature. The primary vertical axis illustrates the total soil water content, composed of three contributing routines: soil box, upper and lower groundwater contents, instinctively in this vertical order, according to section 5.1. The target series is also on this same axis, making a red-blue duality in the middle of the graph.

For the calibration period, the secondary vertical axis presents the climatological inputs in a monthly resolution. The series length made a daily quality impracticable, for precipitation data would be indistinguishable between days and was likely to spoil the graphics for temperature and snow box in the same axis. The soil variables plotted are the monthly picked values described in section 5.2.

For the validation period, however, a daily resolution is feasible for the climatological input. Snowpack thickness now expresses the snow box instead of the accumulated snowmelt. The modeled soil moisture is in monthly resolution due to the necessary compatibility between model and

target series. This duality in resolution, however, elucidates the modeled series quality, emphasizing that the current analysis is for a daily model and does not spoil the graphics' legibility.

6.2 Mato Grosso, Brazil

Figure 15 illustrates the modeling for the calibration period in Mato Grosso. The modeled series is depicted in red, and its good fit to the blue target series is immediately evident. The same broad variation pattern from the target series is noticed: precipitation cools the average temperature in the rainy season, leading to soil moisture build-up; during dry seasons, temperature registers its highest values, resulting in a soil moisture decrease of more than 50%.

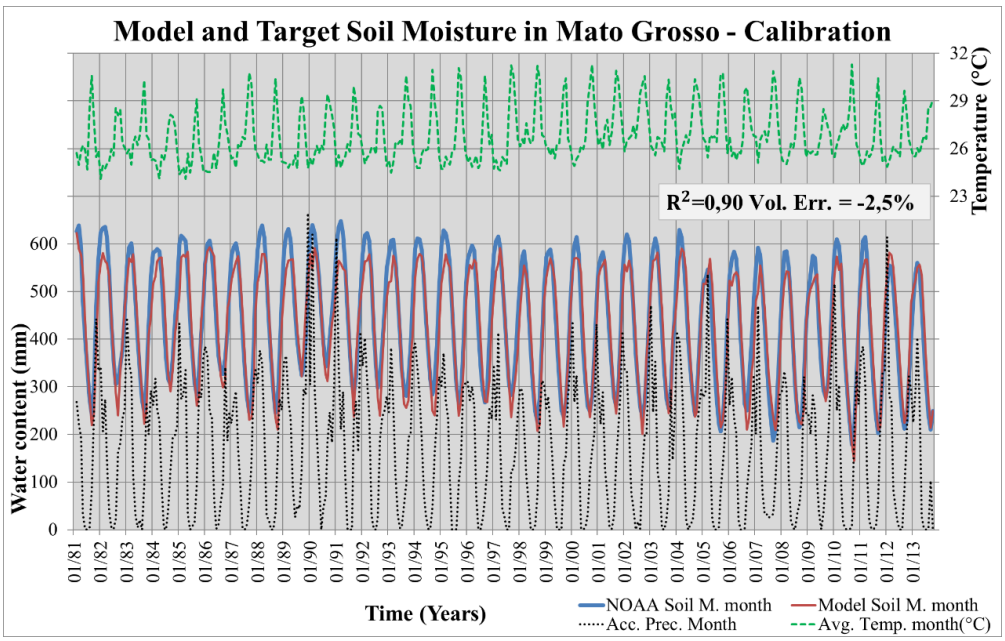

Figure 15: Calibration results for Mato Grosso

The NSE achieved for Mato Grosso in Figure 15 was the highest for this project. The HBV-TR model perfectly mimics the target series between 250 mm to 550 mm of soil moisture. However, the modeled series slightly underestimates the peaking values above that threshold, causing a negative volume error.

Figure 16 depicts the modeling for the validation period, presenting a distinct scenario from calibration. The target series, now consistently below 500 mm, is slightly overestimated during the peaking seasons, as shown by the positive volume error. Moreover, the shape of the second last modeled soil moisture peak does not describe the variations between the wetter months accurately. The NSE drops to 0.85.

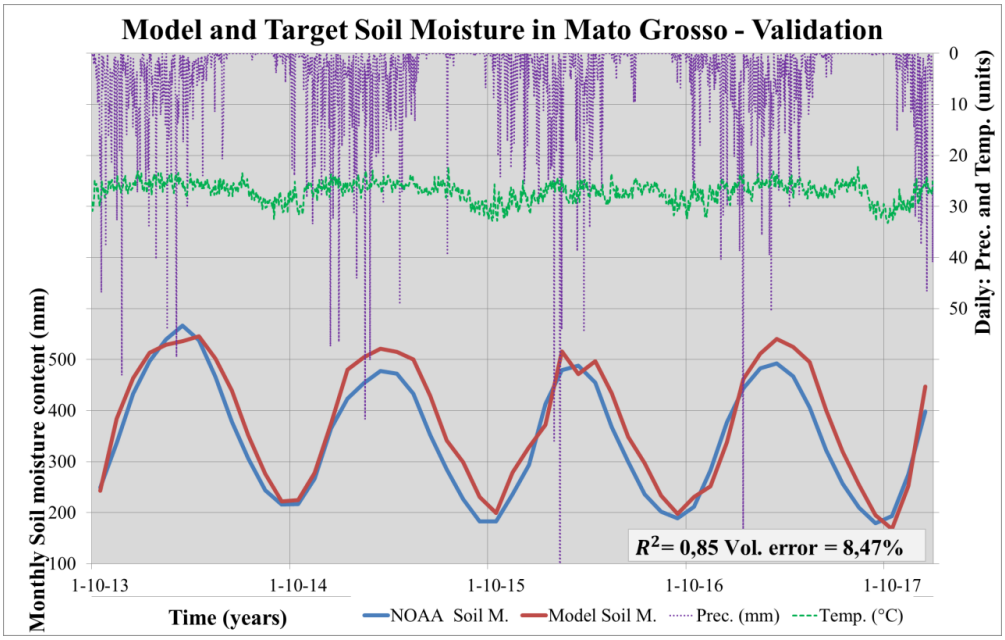

Figure 16: Main validation results for Mato Grosso

The daily weather inputs in Figure 16 show stable patterns and corroborate with the analysis done for the monthly series, being resonant and potentializing the soil moisture variations. The rainy season starts around October, with average daily precipitations easily topping 20 mm, registering showers over 100 mm on two occasions. The average daily temperature varies slowly daily between 23° and 33° year-round, and are consistent with the description given in section 3.1.

Figure 17 emphasizes the relation between precipitation and runoff: rainy seasons with strong showers are accompanied by runoff peaks from 5 to 7.5

mm, while dry seasons lead to accentuated recession curves, with a baseflow around 0.5 mm, thus composing a typical yearly runoff cycle. Evapotranspiration nearly doubles during the rainy season, reaching around 4 mm dropping below 2 mm in the dry season despite daily temperatures of roughly 5°C higher.

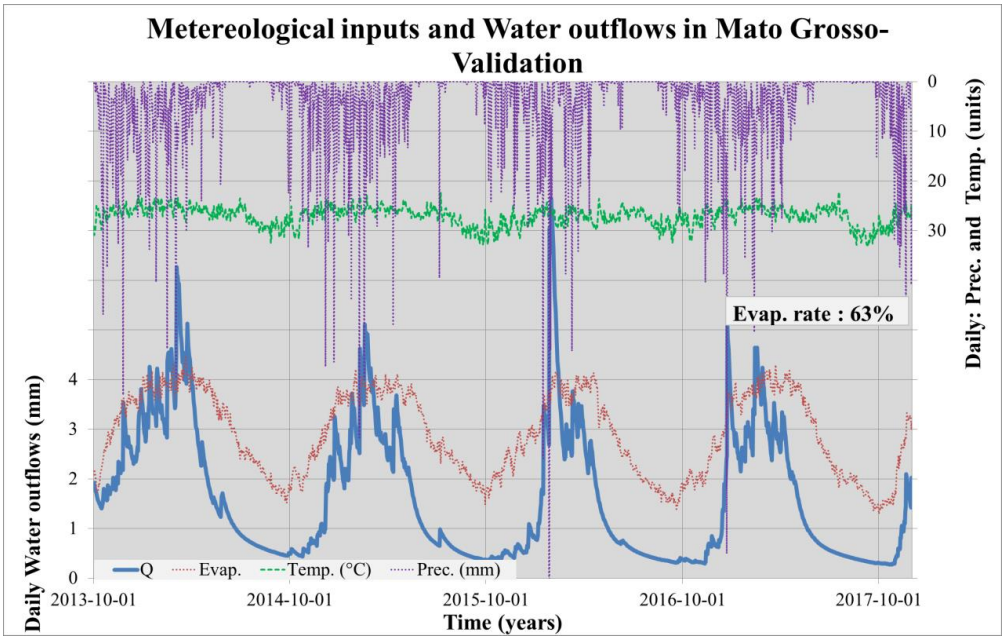

Figure 17: Supplementary validation results for Mato Grosso

6.3 Picardy, France

Figure 18 below conveys the products from calibration for the Picardy region. The modeling for this period shows the influence of snow to be small, not occurring in 1992 and 2008. The modeled water content is mostly composed of the soil moisture box content, represented as the thinner red line *hm month*. During drier seasons, when target values are below 300 mm, this curve is the only significant influence, as seen between summer 1989 and spring 1992. The NSE performance scored 0.88, similar to Mato Grosso.

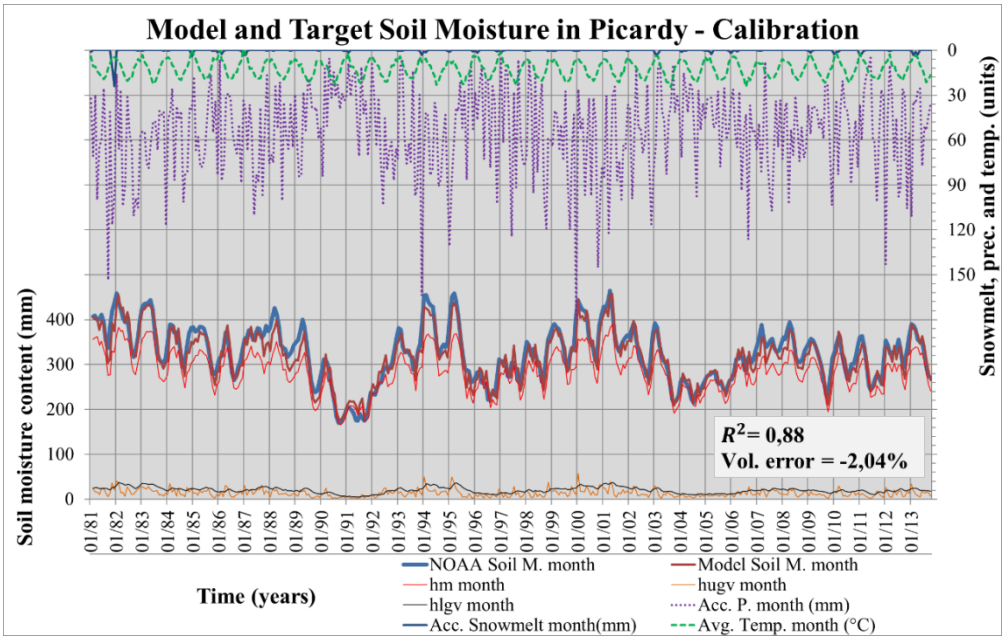

Figure 18: Calibration results for Picardy

Figure 18 shows the response boxes always below 50 mm, but their contributions become substantial for target values above 300 mm. Some highlights of these contributions are the composition of the winter peaks as in 1985, 1994 and 2000. Small underestimations are the trend according to the volume error, markedly occurring during the autumns of 1985, 1988, 1989, and 1996.

Figure 19 below highlights the alternation of predominance between temperature and precipitation for soil moisture values. When an abnormal concentration of rainfall occurred in the summer of 2016, soil moisture values peaked despite the high temperatures. In the next fall, high temperatures until October forced the soil moisture curve below 300 mm, maintaining that level throughout 2017 despite a regular rainfall according to Figure 13. Soil moisture was underestimated during the winter-spring of 2014, while slightly overestimated during the summer of 2016.

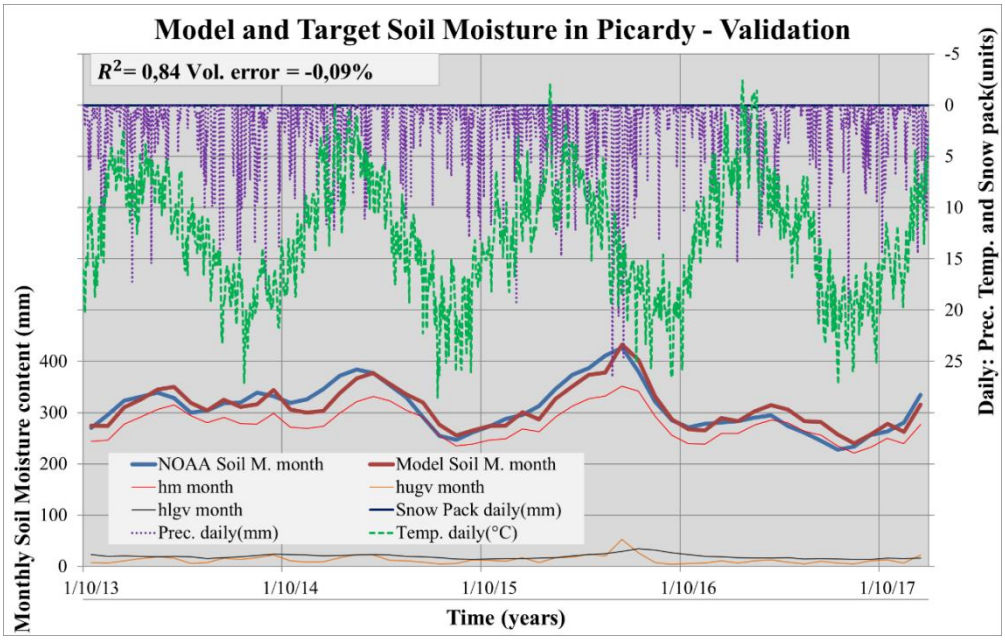

Figure 19: Main validation results for Picardy

Figure 19 above also shows the year of 2015 to be emblematic of the role played by the runoff boxes. When comparing the two modeled red lines, the values for soil moisture decrease faster from spring to late summer, as well as accumulate water more quickly until the following summer of 2016. The NSE parameter was 5% lower than during calibration, while the volume error was insignificant.

The following Figure 20 depicts the water dynamics for Picardy during validation, in which snow played an insignificant part, with temperatures varying from near zero temperatures up to 25°C. Temperature variations are higher than in Mato Grosso in shorter periods of time. The vertical gap between consecutive local maximums and minimums is above 5°C, sometimes reaching a maximum 10°C variation in a couple of days.

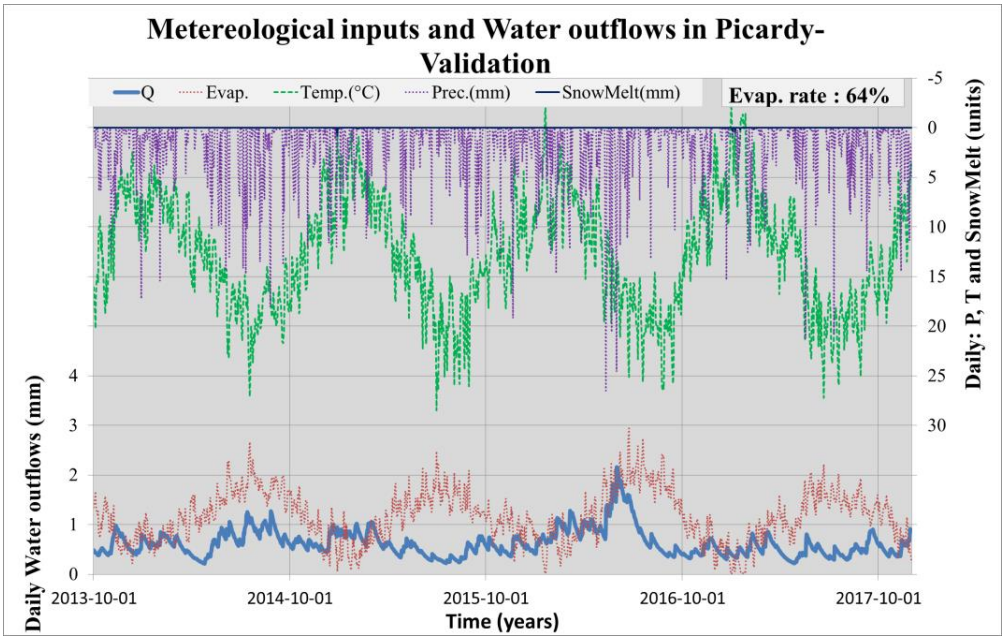

Figure 20: Supplementary validation results for Picardy

Figure 20 displays a proportional relation between evapotranspiration and temperature, as expected. There is synchrony between the evapotranspiration and runoff curves during the summers of 2014 and 2016, contrasting with the drier summers of the odd years. The total evapotranspiration rate is higher than the one registered for Mato Grosso.

The runoff registered in Figure 20 above is continuously close to the baseflow around 0.5 mm, presenting brief recession curves. Regular precipitations that are seldom above 15 mm year-round yield many small peaks in between stronger events. While evapotranspiration commonly ranges from near-zero to 2 mm per day, the runoff presents half of that length, varying between 0.3 and 1 mm, peaking at 2 mm for an unusually rainy period.

6.4 Northwest Iowa, U.S.A.

Figure 21 illustrates the modeled results in Northwest Iowa for calibration. Due to monthly negative average temperatures during winter, the influence of

snowmelt is visible, reaching up to 25 mm as in 1984, 1997 and 2001. The precipitation cycle in Northwest Iowa is well-defined, resembling Mato Grosso, with monthly values varying from near-zero to around 175 mm.

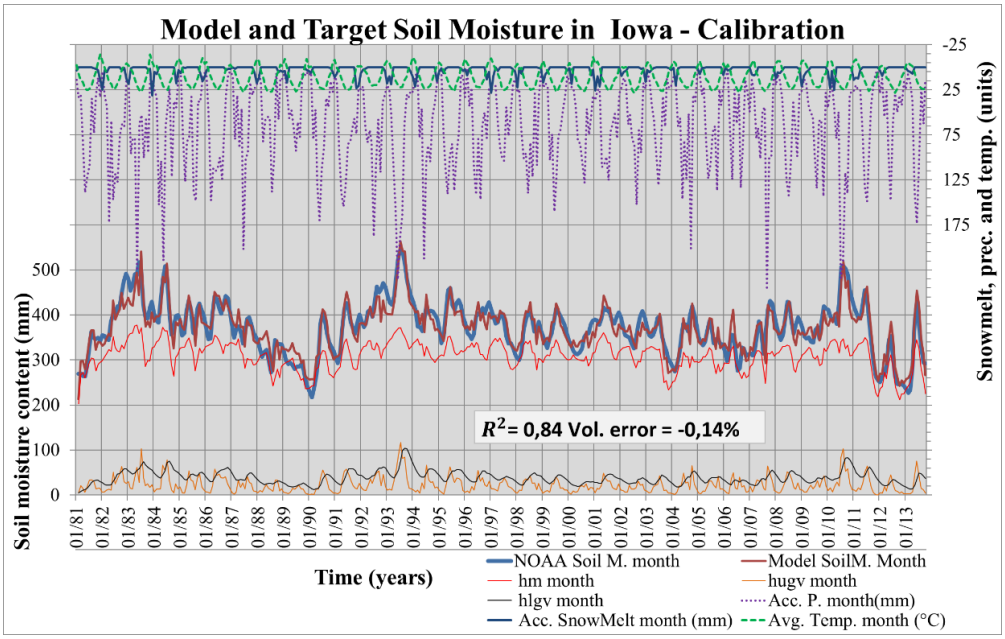

Figure 21: Calibration results for Northwest Iowa

Figure 21 above shows that the modeled soil moisture series grasps the tendencies from the target series, but while it masters extreme variations as between the winter of 1990 and summer 1991 or from 2011 onwards, sometimes it fails to represent minor changes. Some examples are the winter of 1983 or the summer season of 1988 and 1989, which combined result in a lower NSE than for the other areas. As in Picardy, the soil box is the main contributor to soil moisture, but the influence of the response boxes considerably increases for target series over 300 mm.

Figure 22 below is the graphic representing the validation for Northwest Iowa. The snowpack builds up to 10 mm and can be present nearly all- winter long. Gauged precipitation interestingly fits quite well under temperature, more intensive and constant during summer, with two or three showers around 40 mm/day, but nearly ceasing during winter.

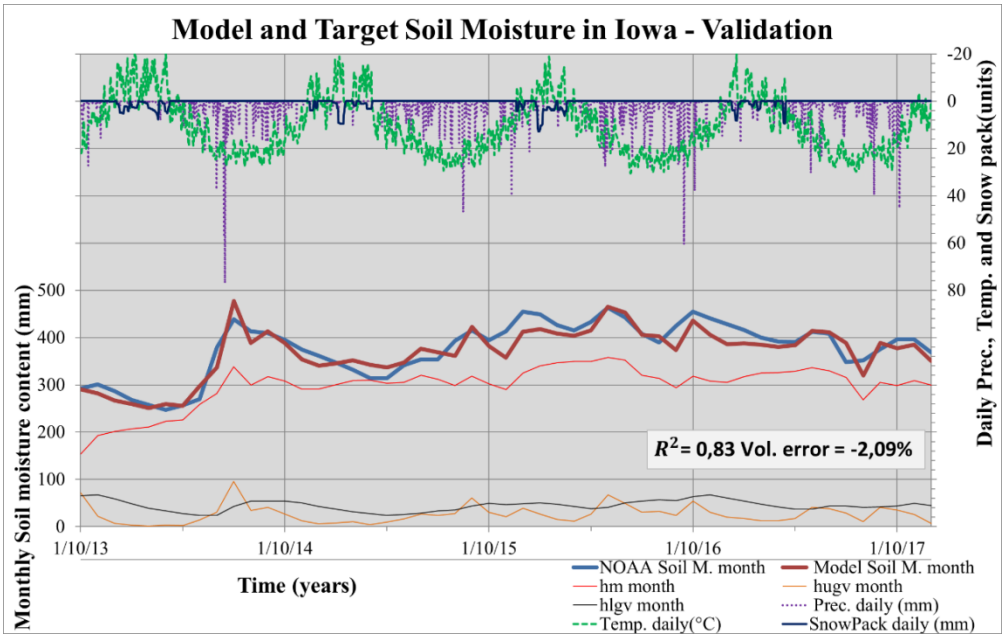

Figure 22: Main validation results for Northwest Iowa

Figure 22 shows how the response boxes improve the modeling for soil moisture in the first two winters. In 2013, the accumulation by the soil box was compensated by both response boxes, thus creating a constant decrease in the modeled series until the beginning of the spring. Between the summers of 2013 and 2014, the response boxes enabled the simulation of two soil moisture crests and a trough, which was not detected by the soil box curve *hm month.*

Figure 23 below highlights the water variables in the region, in which marked peak flows around 2.5 mm occur as a result of summer's intense showers, not being as regular as in Mato Grosso. The snowpack influences the falling limbs in the last two years, nearly doubling the baseflow of 0.5 mm registered in 2013 and 2014. The evaporation rate is significantly lower than the other two basins, for despite its higher registers being superior to Picardy's.

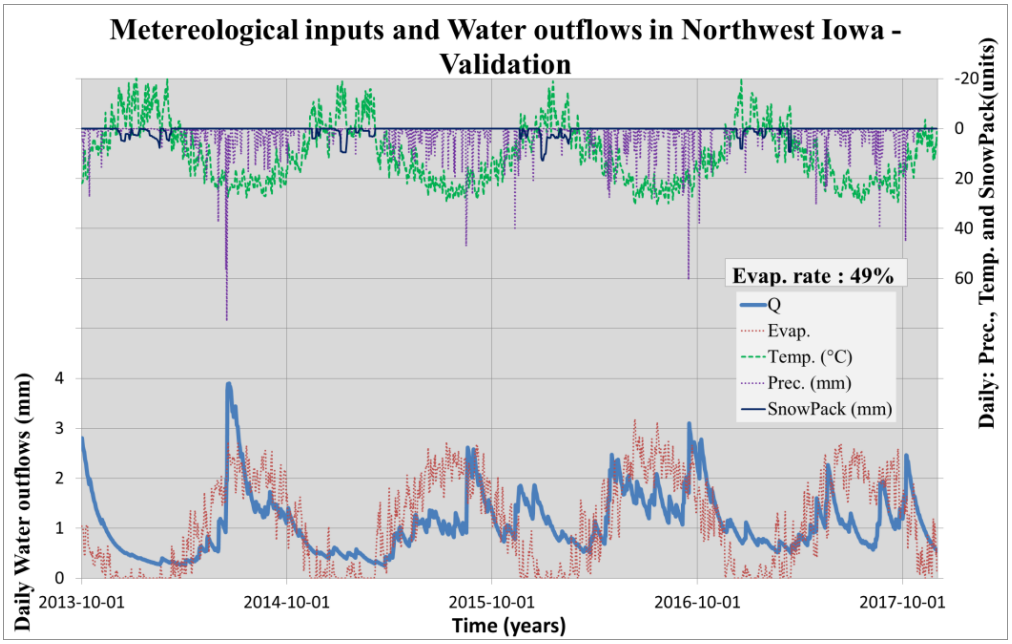

Figure 23: Supplementary validation results for Northwest Iowa

As a supplement to the modeling performance, Figure 24 below illustrates the comparison between the evapotranspiration series yielded by the Leaky-Bucket and HBV-TR models. The visual aspect indicates synchronized series well-distributed throughout the years, and the NSE criterium is even higher than the ones obtained for the soil moisture modeling. From all 50 monthly records, only five modeled values were inferior to the NOAA series.

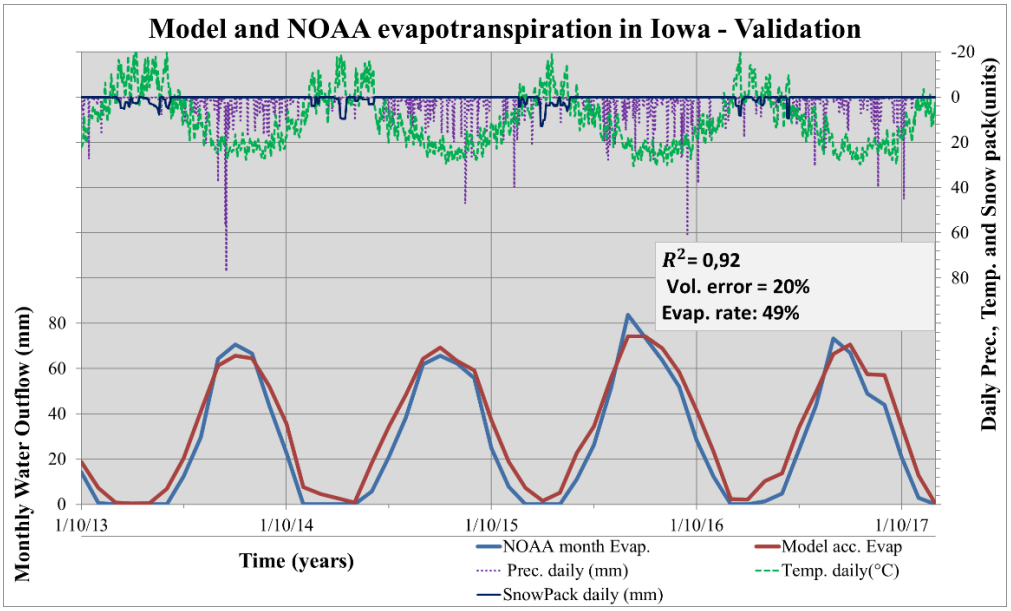

Figure 24: HBV-TR validation through evapotranspiration in Northwest Iowa

A summary of the performance indicators from all HBV-TR modelings, as pointed at section 5.2, can be seen in Table 5 below. The results shown will base the discussion in the next chapter.

AREA / CRITERIA	NSE (calib./ valid.)	Vol. Err. (calib./ valid.; %)	Evap. Rate (val.; %)	Main visual remarks	Model valid. (valid.: *R^2, Vol. Error)	FC (mm)
Mato Grosso	0.9 / 0.85	-2.5 / 8.47	63	Limited accuracy for SM peaks	-	630
Picardy	0.88 / 0.84	-2.04 / -0.09	64	Few underestimations in calibration	-	530
NW Iowa	0.84 / 0.83	-0.14 / -2.09	49	Limited accuracy for quick SM variations	*0.93, 20% * Well-distributed overestim.	430

Table 5: Main performance criteria from the HBV-TR models in all study areas.

7. Discussion

7.1 Mato Grosso, Brazil

The model adaptation for Mato Grosso showed the best NSE performance among all three regions. That, however, can be partially credited to distinct rainy and dry seasons at consistently high temperatures year-round. This fact, combined with similar procedural models used for target and modeled series enabled the only NSE in the 90% level for soil moisture, tolerable volume error and visually a nearly-mirrored modeled series.

Other positive aspects are the shapes of the hydrograph, presenting a marked peak flow and recession curve, along with an evaporation rate much superior to the coldest basin. The inverse proportion observed between temperature and evapotranspiration is evidence that the water available in the soil limits this variable. Otherwise, it would reach much higher values than Picardy, according to Equation 14. The field capacity obtained from Table 4 was 630 mm, below the NOAA limit.

However, the modeling fell a little short for the peaking values of soil moisture, either through general underestimations during calibration or overestimations during validation. This incapacity is at first surprising, given the repetitive, stable yearly cycle in Mato Grosso. During the calibration, the soil box content was always close to the field capacity in the wet months, indicating that either the groundwater recharge or evapotranspiration is excessive when the soil box near saturation (check functions in Table 1).

Given that Figure 24 shows the evapotranspiration from HBV-TR very close to that from the Leaky-Bucket in wet, hot periods, the HBV-TR's groundwater recharge is probably the responsible for this limitation. This analysis also enables the conclusion that *BETA* from HBV-TR is smaller than *b* from the Leaky-Bucket. A possible improvement to avoid running the HBV-TR model near the *FC* values would be deploying the second HBV-TR adaptation, as seen from Figure 18 to Figure 22 for the other regions.

7.2 Picardy, France

Considering the volatility of the local climate explicit in Table 2 and the differences regarding the main variables within soil hydrology between models high lightened in Table 1, the comparison between monthly and daily resolutions between two different models will inevitably bring discrepancies. However, the Picardy model performed nearly as well as Mato Grosso, way above the performance standards.

The Nash-Sutcliff criteria were slightly inferior to the Brazilian, at 0.88 and 0.84, but with a better visual aspect and irrelevant volume errors. The visual aspect is satisfactory overall, being consistent with large and small soil moisture tendencies. The performance improvement due to the response boxes is evident when comparing the modeled series to the soil box curve, *hm month*.

The evapotranspiration rate, higher than the Brazilian and harmonized with temperature, depicts a water-abundant environment, pointing to a realistic basin when compared to Northwest Iowa. The field capacity of 530 mm is satisfactory in comparison to the maximum of 760 mm from NOAA. However, some limited results are also present.

The sporadic misfits pointed during calibration in Figure 18 can be punctual short comes from the calibration and the modeling differences, once there is no drastic meteorological event during autumn in France, and these flaws are not common even in autumns. If the weight distribution depicted better these local targets, the performance for the rest of the series would likely deteriorate. Because the calibration is manual, one must always consider the possibility of better results from a more experienced modeler.

7.3 Northwest Iowa, U.S.A.

The modeling for Northwest Iowa obtained the worst NSE results for both calibration and validation performances, which is natural given it is the most unstable of all three climates in this project. Nonetheless, the performance criteria were all safely above the quality standards, with small volume errors, a consistent NSE record in calibration and validation and an excellent visual

match overall despite some quick target variations, along with a field capacity of 430 mm, way below NOAA's limit.

Apart from these, the hydrograph is consistently in between those observed for Mato Grosso and Picardy. It presents typical peaks after heavy showers which do not amount to yearly hydrographs, for the rainy season is not as concentrated as in the Brazilian state, nor is the modeled snowpack sufficient. The lowest evapotranspiration rate among all areas, 49%, can be attributed to the most prolonged winters, in which there is no evaporation, and to the lower potential evapotranspiration coefficient from the calibration phase, as seen in Table 4, being therefore relatively consistent.

As a product from calibration, hot and cold regions needed corrections around 1.6°C in their state-of-the-art reanalyzed temperature series, coupled with high *Thorn* values. An adverse outcome of this temperature compensation is less snowpack than expected (80 cm according to 3.3, and 25 mm of water, roughly 250 mm of snow, from 6.3). A smaller snowpack is probably responsible for the unnoticed quick variations in the target values pointed in section 6.3, reinforced by the insensitivity of the model to the melt coefficient, set very high for Iowa as seen from Table 4.

When validating the model, the volume error in Figure 24 is unusually high for the figures obtained in this project. However, considering the models are not precisely similar when calculating potential evapotranspiration nor the other vadose zone outflows, this secondary performance parameter in a model validation does not dampen the quality of the visual and NSE performances.

Indeed, the investigation to validate the HBV-TR modeling of the NOAA shows very satisfactory results. The NSE factor obtained was surprisingly high at 0.93, which comes to show that the approximation done by Equation 14 grasps well the same tendencies as the non-linear approach with many variables considered by Thornthwaite in Equation 9. The results from Figure 24 are very reassuring of the methodology applied in this project.

On the shortcomings of the calibration, it is a fact that numerous parameter sets satisfy a modeling. Small imperfections backed by multiple satisfactory

results indicate that the calibration was near an optimum point for the initial direction taken after the sensitivity analysis (Beven 2012).

8. Conclusion and further studies

Describing the theory behind the natural processes of water within the vadose zone was crucial for understanding the unsaturated flow and soil moisture storage. This literature review enabled the comprehension of the models' assumptions, all steps in their calculations, and the differences between them, consolidating the technical basis for the two models.

This project also described the study areas Thomson Reuters put forth, thus depicting the regions regarding their weather, topography, geology, and economic statistics. This background enabled the assimilation of the collected data gathered from NOAA, as well of the importance of the regions in case.

When looking at the input data itself, a description of the methodologies, mostly based on their authors and other hydrologists from NOAA, further aided its assimilation. A model is only as good as its input data, and for that reason, this project evaluated the series' completeness, validity, accuracy, availability, and timeliness. To further guarantee the input soundness, the weather series was completed and selected by their relevance. Graphics supported the consistency of the NOAA series to the study areas background.

According to all the justified efficiency criteria deployed, namely the Nash-Sutcliff efficiency above 0.8, volume error below 10%, comparable evapotranspiration rate, maximum field capacity of 760 millimeters and the visual aspect, the two modeling adaptations based on HBV-TR from 5.1 can be considered successful. The small deviations are within the tolerance margin and are plausible given two different models and hydrologists. So many acceptable modeling approaches for soil moisture depict the fact that all have their limitations (Palmer 1965).

The more straightforward adaptation deployed for Mato Grosso considering only the soil moisture box in the HBV-TR model proved to be very close to the dynamics within the routine from the Leaky-Bucket, validating this approach. The lower performance when modeling for values near field capacity points to more efforts in deploying the second HBV-TR adaptation for these cases.

The addition of the response boxes to the model setup for the two other regions demonstrated to be positive. HBV-TR's enhanced resolution in climates that are unstable on a daily basis did not, however, compromise the capacity to express monthly or seasonal behaviors. The modeling performances here achieved are safely above the thresholds established by Thomson Reuters.

This project shows substantial evidence that soil moisture can be modeled by HBV-TR with a daily resolution, presenting the potential to become another product in Thomson Reuters's forecast portfolio. This way, Thomson Reuters can provide a tool for farm producers to increase their productivity and consequently to lower food price, stabilizing food markets and meeting global demands.

References

BARBARISI, B.F., PILAU, F.G., MARIN, F.R., ASSAD, E.D. and PINTO, H.S., 2006. Estimativa da temperatura do ar para os estados de Mato Grosso do Sul, Mato Grosso, Goiás e Tocantins a partir do uso de imagens de Radar. In: Embrapa Informática Agropecuária-Resumo em anais de congresso (ALICE*)* 2006, *Congresso Brasileiro de Meteorologia*, 2006. Florianópolis: Sociedade Brasileira de Meteorologia.

BERGSTRÖM, S., 1992. *The HBV model: Its structure and applications: Report No. 4.*[pdf] Norrköping: Swedish Meteorological and Hydrological Institute. Available at: <https://www.smhi.se/polopoly_fs/1.83592!/Menu/general/extGroup/attachmentColHold/mainCol1/file/RH_4.pdf> [Accessed on April 08, 2018]

BEVEN, K.J., 2012. *Rainfall-runoff modelling: the primer.*[e-book] Chichester, West Sussex ; Hoboken, NJ : Wiley-Blackwell, 2012; 2nd ed. Available through: Lund University Library website <http://ludwig.lub.lu.se/login?url=http://search.ebscohost.com/login.aspx?direct=true&db=cat01310a&AN=lovisa.004268855&site=eds-live&scope=site http://ludwig.lub.lu.se/login?url=https://www.dawsonera.com/abstract/9781119951018> [Accessed April 9, 2018]

BLONDEL, J.F.P., SHENNAN, J.H. and ET AL, 2018. *France*. [online] Available at: <https://www.britannica.com/place/France/The-great-lowlands#ref468810> [Accessed on February 9, 2018]

BOLTEN, J.D., CROW, W.T., XIWU ZHAN, JACKSON, T.J. and REYNOLDS, C.A., 2010. Evaluating the Utility of Remotely Sensed Soil Moisture Retrievals for Operational Agricultural Drought Monitoring. *IEEE Journal of Selected Topics in Applied Earth Observations and Remote Sensing*, **3**(1), pp. 57-66.

CHEN, M., XIE, P., JANOWIAK, J.E. and ARKIN, P.A., 2002. Global land precipitation: A 50-yr monthly analysis based on gauge observations. *Journal of Hydrometeorology*, **3**(3), pp. 249-266.

EMBLETON, C., 1984. *Geomorphology of Europe.* London: Macmillan.pp. 153-161

EMBRAPA, 1982. *Levantamento de reconhecimento de media intensidade, avaliacao da aptidao agricola das terras e indicacao de culturas em areas homogeneas de solos de alguns municipios do sudoeste do Estado de Mato Grosso.* [e-book] Rio de Janeiro: EMBRAPA. Available through: EMBRAPA publications website <https://www.embrapa.br/solos/busca-de-publicacoes/-/publicacao/336051/levantamento-de-reconhecimento-de-media-intensidade-avaliacao-da-aptidao-agricola-das-terras-e-indicacao-de-culturas-em-areas-homogeneas-de-solos-de-alguns-municipios-do-sudoeste-do-estado-de-mato-grosso> [Accessed March 10, 2018]

ENCYCLOPAEDIA BRITANNICA, 1820. *Supplement to the fourth, fifth and sixth editions of the Encyclopaedia Britannica. With preliminary dissertations on the history of the sciences.* Edinburgh: Archibald Constable.

ENCYCLOPÆDIA BRITANNICA, January 11, 2018-last update, Iowa [[Online]. Available at: <https://www.britannica.com/place/Iowa-state> [Accessed February 09, 2018].

ENCYCLOPÆDIA BRITANNICA, 2016. *Picardy.* [online]. Available at: <http://academic.eb.com/levels/collegiate/article/59899> [February 10, 2018]

FAN, Y. and VAN DEN DOOL, H., 2004. Climate Prediction Center global monthly soil moisture data set at 0.5 resolution for 1948 to present. *Journal of Geophysical Research: Atmospheres,* **109**(D10),.

FARM MANAGEMENT, May 15, 2018-last update, 5 methods of manipulating soil moisture levels. Available at: <http://www.farmmanagement.pro/5-methods-of-manipulating-soil-moisture-levels/.> [Accessed May 15, 2018]

FETTER, C.W., 2014. *Applied hydrogeology.* Fourth ed. Edimburgh: Pearson Education.

GOOGLE EARTH 7.1.8.3036, 2017a. *Northwest Iowa.* 43° N 95° W

GOOGLE EARTH, 7.1.8.3036, 2017b. *Picardy Region. 49°37′ N 2°38′ E*

GOOGLE EARTH, 2017c. *State of Mato Grosso. 13° S 56° W*

HUANG, J., VAN DEN DOOL, HUUG M and GEORGARAKOS, K.P., 1996. Analysis of Model-Calculated Soil Moisture over the United States (1931–1993) and Applications to Long-Range Temperature Forecasts. *Journal of Climate*, **9**(6), pp. 1350-1362.

HUUG VAN DEN DOOL, JIN HUANG and YUN FAN, 2003. Performance and analysis of the constructed analogue method applied to U.S. soil moisture over 1981–2001. *Journal of Geophysical Research - Atmospheres*, **108**(D16), pp. 8617.

IBGE, 2017-last update. *Panorama de Mato Grosso*. [online] Available at: <https://cidades.ibge.gov.br/brasil/mt/panorama> [Accessed April 06, 2018].

IBGE, 2016. *Produção Agrícola Municipal : culturas temporárias e permanentes.* 43. Rio de Janeiro: IBGE.

IBGE, 2010. *Atlas nacional do Brasil Milton Santos / IBGE, Diretoria de Geociências.* -. Rio de Janeiro: IBGE.

JÓDAR, J., CARPINTERO, E., MARTOS-ROSILLO, S., RUIZ-CONSTÁN, A., MARÍN-LECHADO, C., CABRERA-ARRABAL, J., NAVARRETE-MAZARIEGOS, E., GONZÁLEZ-RAMÓN, A., LAMBÁN, L., HERRERA, C. and GONZÁLEZ-DUGO, M., 2018. Combination of lumped hydrological and remote-sensing models to evaluate water resources in a semi-arid high altitude ungauged watershed of Sierra Nevada (Southern Spain). *Science of Total Environment* [e-journal] 625, pp.285-300. http://doi.org/10.1016/j.scitotenv.2017.12.300

KRAUSE, P., BOYLE, D.P. and BÄSE, F., 2005. Comparison of different efficiency criteria for hydrological model assessment. *Advances in Geosciences*, **5**, pp. 89-97.

LICKER, R., KUCHARIK, C.J., DORÉ, T., LINDEMAN, M.J. and MAKOWSKI, D., 2013. Climatic impacts on winter wheat yields in Picardy,

France and Rostov, Russia: 1973–2010. *Agricultural and Forest Meteorology*, **176**, pp. 25-37.

MAPS OF THE WORLD, 2017. *Physical map of Iowa*. [image online] Available at: <https://www.mapsofworld.com/usa/states/iowa/physical-map-of-iowa.html> [Acessed May 08, 2018].

METEO FRANCE, 2017-last update, Les climat en France. Available at: <http://www.meteofrance.fr/climat-passe-et-futur/climat-en-france/le-climat-en-metropole#> [Accessed February 19, 2018].

MORIASI, D.N., ARNOLD, J.G., VAN LIEW, M.W., BINGNER, R.L., HARMEL, R.D. and VEITH, T.L., 2007. Model evaluation guidelines for systematic quantification of accuracy in watershed simulations. *Transactions of the ASABE*, **50**(3), pp. 885-900.

NOAA, 2018-last update, *Climate of Iowa* [pdf] Available at: <http://www.crh.noaa.gov/Image/dvn/downloads/Clim_IA_01.pdf> [Accessed February 11, 2018].

NOAA, Aug 22, 2002-last update, *Explanation* [online]. Available at: <http://www.cpc.ncep.noaa.gov/soilmst/descrip.htm> [Accessed February 11, 2018].

OXFORD WORLD ENCYCLOPEDIA, 2004. *Picardy [Picardie]* [online]. Available at: <http://www.oxfordreference.com/view/10.1093/acref/9780199546091.001.0001/acref-9780199546091-e-9030> [Accessed April 08,2018]

PALMER, W.C., 1965. *Meteorological drought.* 45. Washington D.C.: U.S. Government Printing Office.

PRIOR, J.C. and IOWA, G.S., 1976. *A Regional Guide to Iowa Landforms. Iowa Geological Survey Educational Series 3.*

SAHA, S., MOORTHI, S., PAN, H., WU, X., WANG, J., NADIGA, S., TRIPP, P., KISTLER, R., WOOLLEN, J. and BEHRINGER, D., 2010. The

NCEP climate forecast system reanalysis. *Bulletin of the American Meteorological Society*, **91**(8), pp. 1015-1058.

SCHULZKE, D. and KAULE, G., 2001. Agro-Ecological Classification and Spatial Demarcation of Western Europe. *Archives of Agronomy & Soil Science*, **46**(5), pp. 385.

SHUKLA, M.K., 2011. *Soil hydrology, land use and agriculture. [Elektronisk resurs] : measurement and modelling.* Wallingford : CAB International, 2011.

SMHI, 2015-last update, *HBV* [online] Available at: <https://www.smhi.se/en/research/research-departments/hydrology/hbv-1.90007> [Accessed Mar 08, 2018].

SOUZA, A.P., MOTA, L.L., ZAMADEI, T., MARTIN, C.C., ALMEIDA, F.T. and PAULINO, J., 2013. Classificação climática e balanço hídrico climatológico no Estado de Mato Grosso. *Nativa*, **1**(1), pp. 34-43.

STATE ADMINISTRATION OF MATO GROSSO, 2015-last update, *Geografia*. [online] Available at: <http://www.mt.gov.br/geografia> [Accessed April 06, 2018].

THOMSON REUTERS, 2018. *Input data provided by Thomson Reuters.* [e-mail] (Personal communication, January 30, 2018)

THORNTHWAITE, C.W., 1948. An approach toward a rational classification of climate. *Geographical Review*, **38**(1), pp. 55-94.

TUCCI, C.E.M. and SILVEIRA, ANDRÉ L L DA, 2009. *Hidrologia: Ciência e Aplicação.* 4 edn. Porto Alegre: UFGRS.

Larsson, R., 2017. Water Movement in Soil. *VVRN 010 Rainfall Runoff modelling.* [online via internal VLE] Lund University. Available at: <http://www.tvrl.lth.se/fileadmin/tvrl/files/vvr140/Lecture_water_in_soil_2017.pdf > [Accessed April 23, 2018]

U.S. DEPARTMENT OF AGRICULTURE, 1955. *The Yearbook of agriculture.* Washington, DC: US Gov.Print.Off.

UNITED NATIONS, 2015Transforming our world : the 2030 Agenda for Sustainable Development
, 2015, United Nations, pp. 16-18.

WIKISOFT, 2008. *700x700 CARTE FRANCE GEO Regions R1*.

YEIK, T., Mar 04, 2014-last update, Maximize irrigation benefits by managing soil moisture. Available at: <https://www.progressiveforage.com/forage-production/irrigation/maximize-irrigation-benefits-by-managing-soil-moisture> [Accessed April 24, 2018].

YUN FAN and HUUG VAN DEN DOOL, 2008. A global monthly land surface air temperature analysis for 1948–present. *Journal of Geophysical Research - Atmospheres*, **113**(D1), pp. D01103.